nature communications

Article

https://doi.org/10.1038/s41467-025-58277-5

A fungal pathogen suppresses host leaf senescence to increase infection

Received: 12 July 2024

Accepted: 14 March 2025

Published online: 24 March 2025

Check for updates

Yue Li[1,2,4], Xiangru Qu[1,2,4], Wenjuan Yang[1,2], Qin Wu[1,2], Xiaodong Wang[3], Qiantao Jiang[1,2], Jian Ma[1,2], Yazhou Zhang[1,2], Pengfei Qi[1,2], Guoyue Chen[1,2], Youliang Zheng[1,2], Xiaojie Wang[3] ✉, Yuming Wei[1,2] ✉ & Qiang Xu[1,2] ✉

Phytopathogens such as *Puccinia striiformis* f. sp. *tritici* (*Pst*) induce pigment retention at pathogen infection sites. Although pigment retention is commonly observed in diverse pathosystems, its underlying physiological mechanism remains largely unclear. Herein, we identify and characterize a wheat leaf senescence gene, *TaSGR1*, which enhances resistance against *Pst* by promoting leaf senescence and H_2O_2 accumulation while inhibiting photosynthesis. Knockout of *TaSGR1* (STAYGREEN) in wheat increases pigment retention and plant susceptibility. Pst_TTP1 (TaTrx-Targeting Protein 1), a secreted rust fungal effector critical for *Pst* virulence, binds to the plastidial thioredoxin TaTrx (Thioredoxin), preventing its translocation into chloroplasts. Within the chloroplasts, TaTrx catalyzes the transformation of TaSGR1 oligomers into monomers. These TaSGR1 monomers accumulate in the chloroplasts, accelerating leaf senescence, H_2O_2 accumulation, and cell death. The inhibition of this oligomer-to-monomer transformation, caused by the failure of TaTrx to enter the chloroplast due to Pst_TTP1, impairs plant resistance against *Pst*. Overall, our study reveals the suppression of redox signaling cascade that catalyzes the transformation of TaSGR1 oligomers into monomers within chloroplasts and the inhibition of leaf chlorosis by rust effectors as key mechanisms underlying disease susceptibility.

Plant diseases caused by pathogens, such as filamentous fungi, oomycetes, and bacteria, are among the greatest threats to plant survival and crop productivity in nature[1,2]. Complex relationships between plant immunity and pathogenesis mechanisms, together with abiotic factors, determine the various modes of plant–pathogen interactions. Biotrophic pathogens feed on live plant cells, whereas necrotrophic pathogens kill plant cells to absorb nutrients. A third group, known as hemibiotrophic pathogens, initially accesses nutrients from living tissue before switching to a necrotrophic phase[3,4]. During infection, these pathogens secrete effector proteins into plant cells to manipulate the host's functions and cause disease. Although many pathogenic effectors have been well-documented to target plant immune-related components to inhibit host immunity, some effectors create a more favorable environment at infection sites for fungal growth and disease development[5–7]. A typical example is the bacterial effector AvrE from *Pseudomonas syringae*, which, as a water-soaking inducer, has been shown to alter ABA signaling and stomatal closure to create a water-rich apoplastic environment for pathogen propagation[8]. In another bacterial pathogen, *Ralstonia solanacearum*, the effector protein RipI has been shown to interact with plant glutamate decarboxylases to hijack plant metabolism and support bacterial growth[9]. In the presence of several obligate biotrophic or hemibiotrophic fungal pathogens,

[1]State Key Laboratory of Crop Gene Exploration and Utilization in Southwest China, Chengdu, Sichuan, China. [2]Triticeae Research Institute, Sichuan Agricultural University, Chengdu, Sichuan, China. [3]State Key Laboratory for Crop Stress Resistance and High-Efficiency Production, College of Plant Protection, Northwest A&F University, Yangling, Shaanxi, China. [4]These authors contributed equally: Yue Li, Xiangru Qu. ✉e-mail: wangxiaojie@nwsuaf.edu.cn; ymwei@sicau.edu.cn; xuqiang1264700418@163.com

spots of pigment retention, known as green islands, are commonly observed at infection sites and are surrounded by yellow, senescing tissue[10]. The formation of green islands is usually considered to favor the uptake of nutrients by pathogens by prolonging the life of host tissues, thereby extending period of pathogen reproduction or sporulation[11]. However, to date, the physiological mechanism by which fungi induce the formation of green islands to sustain biotrophy remains poorly understood.

Leaf senescence is not a passive physiological phenomenon but rather a developmentally programmed process that is coordinated and modulated by biotic and abiotic factors[12,13]. *Verticillium dahliae* has been shown to subtly manipulate leaf senescence, increasing the availability of nutrients to senescing leaves during its necrotrophic stage[14]. Conversely, biotrophic pathogens such as the wheat stripe rust pathogen (*Puccinia striiformis* f. sp. *tritici*, *Pst*), an important obligate parasitic filamentous pathogen affecting wheat worldwide, can only survive on living tissue, keeping the host alive completing its life cycle[15]. The rapid accumulation of reactive oxygen species (ROS), localized cell death, and leaf senescence constitute the host's response at infection sites to prevent nutrient uptake by biotrophic pathogens and inhibit their further proliferation[16]. A prime example of senescence-associated resistance is that mediated by plant resistance genes, including the rust resistance genes *Yr36* and *Lr67*[17]. Yr36 functions by interacting with and disintegrating the photosystem II (PSII) PsbO component, ultimately accelerating leaf chlorosis and cell death[18]. Lr67 has been shown to exert a negative effect on glucose uptake by heterodimerization, leading to leaf tip senescence and necrosis[19].

The loss of chlorophyll (Chl) and degradation of the photosynthetic apparatus are prominent features of senescence, followed by the decomposition of macromolecules such as proteins, nucleic acids, and lipids. The Chl metabolism not only regulates photosynthesis and nutrient recycling but also influences the defense response in plants[20,21]. Porphyrin compounds, which are intermediates of Chl, act as potential cell phototoxins, inducing ROS accumulation and hypersensitive response (HR)[22,23]. The loss of ferredoxin-dependent glutamate synthase 1 during Chl biosynthesis has been shown to lead to ROS accumulation and confer broad-spectrum resistance to bacterial blight in rice[24]. In *Arabidopsis*, increased expression of STAYGREEN proteins accelerates cell death, whereas decreased expression suppresses it[25,26]. Another study demonstrated that a loss-of-susceptibility mutation of CsSGR in *Cucumis sativus* conferred broad-spectrum resistance against fungal anthracnose, downy mildew, and bacterial angular leaf spot by regulating Chl breakdown and ROS accumulation[27]. The silencing of wheat pheophorbide a oxygenase, which is involved in Chl catabolism, has been shown to cause leaf cell death and enhance tolerance to *Pst*[28]. Several studies have provided new insights into Chl biosynthesis and breakdown associated with pathogen effectors. The bacterial effector SDE1 from *Candidatus* Liberibacter asiaticus was identified as an inhibitor of papain-like cysteine proteases and has been shown to contribute to the progression of citrus greening disease, possibly by accelerating senescence in citrus[29]. In hemibiotrophic fungi, the effector PevD1 from *V. dahliae* induces leaf senescence by promoting ORE1-mediated ethylene biosynthesis, increasing nutrient uptake in aging tissues during the necrotrophic stage[30]. The necrotrophic fungus *Rhizoctonia solani* can manipulate Chl biosynthesis and degradation to absorb nutrients from dead cells and extend infection[31]. However, compared to other effectors, the molecular mechanisms by which effector proteins regulate leaf senescence in the biotrophic fungus *Pst* remain insufficiently explored.

In this study, we functionally identified a putative *Pst* effector, Pst_TTP1, which disrupts chloroplast function to suppress leaf senescence at infection sites. This fungus-secreted effector, which is crucial for *Pst* virulence, performs this function by targeting and preventing wheat thioredoxin (TaTrx) from entering the chloroplasts, thereby likely suppressing the redox signaling cascade that catalyzes the transformation of TaSGR1 oligomers into monomers within these organelles, ultimately inhibiting the activity of TaSGR1. CRISPR–Cas9 inactivation of *TaSGR1* or *TaTrx* reduced wheat resistance to *Pst*. However, *TaSGR1* expression was found to contribute to chloroplast-derived ROS accumulation and improved disease resistance. Additionally, TaSGR1 monomers enhanced resistance against *Pst* by promoting leaf senescence and H_2O_2 accumulation while inhibiting photosynthesis. Overall, the inhibition of redox signaling delivery to chloroplasts by pathogen virulence factors represents a pathogenic strategy to manipulate plant senescence and support fungal nutrition.

Results

TaSGR1 enhances Chl breakdown in plants

The transcriptome of wheat infected with *Pst* was screened and analyzed to better understand the role of Chl-related genes in resistance to this pathogen[32]. Among the differentially expressed genes associated with Chl metabolism and biosynthesis in *Pst*-infected wheat leaves, TaSGR1 was identified as a highly expressed gene encoding a chloroplast-targeting protein with a STAYGREEN domain involved in Chl breakdown (Supplementary Fig. 1a). Owing to 97% similarity in nucleotide sequences among three copies of *TaSGR1* (Supplementary Fig. 1b), we cloned only *TaSGR1-5B* from the cDNA of Chinese Spring plants. Variations in the coding sequence (CDS) of *TaSGR1-5B* mainly resulted in 2 haplotypes with 17 single-nucleotide polymorphisms among wheat cultivars (Supplementary Fig. 2a). To determine its function, *TaSGR1-5B* was fused with a green fluorescent protein (GFP) construct driven by the CaMV35s promoter for transient expression in wheat protoplasts. Mlp107772 (CTP1), has previously been reported to localize in chloroplasts, was used as a marker protein for chloroplast localization[33]. In cells expressing TaSGR1-GFP, GFP signals were specifically observed in the chloroplast, whereas TaSGR1$^{\Delta cTP}$-GFP (lacking chloroplast-targeting peptides, cTP) was distributed throughout the entire cell (Supplementary Fig. 1c).

To further determine the role of TaSGR1 in Chl metabolism, it was transiently expressed in *N. benthamiana*. The results showed accelerated leaf yellowing and Chl breakdown in tobacco cells expressing TaSGR1-GFP but not in leaves expressing TaSGR1$^{\Delta cTP}$-GFP (Supplementary Fig. 1d). The maximal PSII activity parameter (Fv/Fm) and nonphotochemical quenching (NPQ) decreased in tobacco cells expressing TaSGR1-GFP (Supplementary Fig. 1e). The expression levels of TaSGR1-GFP expression also resulted in ROS bursts and cell death (Supplementary Fig. 1f). Next, transgenic wheat lines overexpressing *TaSGR1-5B* (*TaSGR1*OE) were generated. The expression levels of *TaSGR1* were fourfold and fivefold higher in two T_2 lines, *TaSGR1*OE#L1 and *TaSGR1*OE#L3, respectively, and the YFP-tagged TaSGR1 protein was also detected, indicating successful expression of TaSGR1 in the *TaSGR1*OE plants (Supplementary Fig. 3a, b). Accelerated leaf yellowing, photosynthetic inhibition, and the high expression of senescence-related genes were observed in *TaSGR1*OE plants, which is consistent with the results obtained in *N. benthamiana* (Supplementary Fig. 3c–e). Chloroplast suborganelle structures were decomposed in *TaSGR1*OE plants, indicating that TaSGR1 accelerated chloroplast degeneration and induced leaf yellowing and senescence (Supplementary Fig. 3f). In the transgenic *TaSGR1*OE lines, the thousand grain weight reduced by 10% than that of Fielder plants under greenhouse conditions (Supplementary Fig. 3g). Overall, these results indicate that *TaSGR1* expression contributes to leaf senescence and ROS accumulation.

TaSGR1 positively regulates wheat resistance to *Pst*

To understand the role of TaSGR1 in wheat–*Pst* interaction, its expression was first evaluated during this interaction. All three TaSGR1 homeologs, i.e., *TaSGR1-5A*, *TaSGR1-5B*, and *TaSGR1-5D*, exhibited an eightfold upregulation upon infection with *Pst* at 24 h post-infection

https://doi.org/10.1038/s41467-025-58277-5

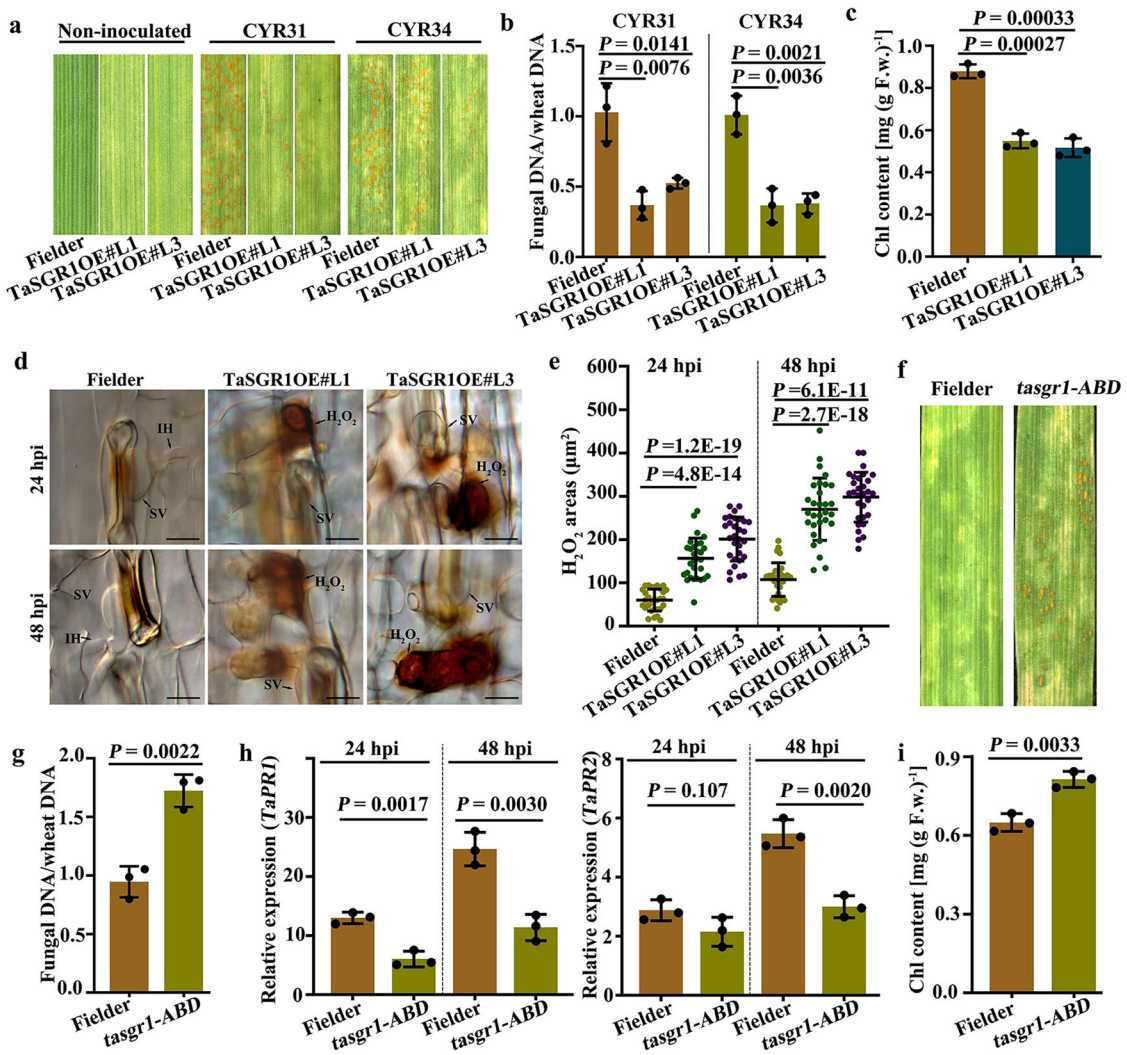

Fig. 1 | TaSGR1 positively regulates wheat resistance to *Pst*. **a** *TaSGR1*OE and Fielder plants were inoculated with *Pst* CYR31 and CYR34, and disease phenotypes were observed at 14 dpi. **b** The *Pst*/wheat biomass ratio in infected leaves at 120 hpi was measured using qPCR. **c** Chl contents decreased in *Pst* CYR31-infected *TaSGR1*OE plants at 5 dpi. **d** H_2O_2 accumulation was observed after DAB staining in the leaves of *Pst* CYR31-infected *TaSGR1*OE wheat plants at 24 or 48 hpi. Bar = 20 mm. SV substomatal vesicle, IH infectious hyphae. **e** Quantification of infection areas containing H_2O_2 in Fielder and *TaSGR1*OE plants infected with *Pst* CYR31 at 24 and 48 hpi. Means ± standard deviation (SD) were calculated from 30 infection sites across three independent biological replicates from three leaf samples of different plants. The *P* value was determined using a two-tailed unpaired Student's *t* test. **f** Fielder and *tasgr1-ABD* plants were inoculated with *Pst* CYR23, and disease phenotypes were observed at 14 dpi. **g** The *Pst* biomass in infected leaves was measured using qPCR. **h** Relative expression of the marked defense-related genes in *tasgr1-ABD* plants at 0 and 24 hpi with *Pst* CYR23. Transcript levels were confirmed via qPCR and normalized to *TaEF1a*. **i** Chl contents in *Pst* CYR23-infected *tasgr1-ABD* plants decreased at 5 dpi. In (**b**, **c**, **g**, **h**, and **i**), mean values and SD were determined ($n = 3$ biologically independent samples). The *P* value was determined using a two-tailed unpaired Student's *t* test. Source data are provided as a Source Data file.

(hpi) (Supplementary Fig. 4). Two haplotypes of *TaSGR1-5B* from Chinese Spring and Fielder plants were transiently overexpressed to detected their function. Compared with the control, both haplotypes enhanced plant resistance to *Pst* upon inoculation with *Pst* CYR34, indicating that these two haplotypes have identical efficiencies (Supplementary Fig. 2c). The resistance of *TaSGR1*OE plants to *Pst* was further evaluated by inoculating them with virulent *Pst* CYR31 and CYR34. Fielder plants developed numerous urediniospore pustules and showed no obvious HR at 14 days post-infection (dpi), whereas *TaSGR1*OE plants developed sporadic urediniospore pustules and HR (Fig. 1a). Compared with Fielder, the *Pst* biomass of CYR31 and CYR34 was significantly reduced by 50–60% at 120 hpi in *TaSGR1*OE#L1 and #L3 plants (Fig. 1b). Interestingly, the Chl content in *TaSGR1*OE plants leaves was significantly decreased at 5 dpi (Fig. 1c). Upon *Pst* CYR31 infection, 3,3′-diaminobenzidine (DAB) staining showed higher H_2O_2 accumulation in *TaSGR1*OE#L1 and #L3 plants, and trypan blue staining revealed higher cell mortality in *TaSGR1*OE than in Fielder plants at 5 dpi (Fig. 1d, e and Supplementary Fig. 5a). The transcript levels of *TaPR1* and *TaPR2* were increased by two- to threefold at 24 and 48 hpi in the *TaSGR1OE*#L1 and #L3 plants compared with Fielder plants (Supplementary Fig. 5b). Additionally, hyphal length and infection areas at 24 and 48 hpi decreased in *TaSGR1*OE plants (Supplementary Fig. 5c, d).

To provide broader insights into the resistance mechanisms of TaSGR1, we conducted RNA sequencing (RNA-seq) analysis with infected wheat leaves of *TaSGR1*OE#L1 and #L3 plants that were inoculated with *Pst* CYR34 and collected at 24 hpi. A total of 388 upregulated and 812 downregulated differentially expressed genes (DEGs) with at least twofold changes were identified in wheat leaves of *TaSGR1*OE plants compared to the *Pst*-inoculated Fielder plants

(Supplementary Data 1). Gene ontology (GO) analysis showed that DEGs were significantly enriched for genes functionally related to chloroplastic activity (chloroplast thylakoid, thylakoid, etc.), oxidoreductase activity (iron–sulfur cluster binding, cell redox homeostasis, etc.), and cytoplasm terms (Supplementary Data 2, Supplementary Fig. 6). Interestingly, eight of the upregulated DEGs in *TaSGR1*OE plants encode putative NBS-LRR proteins, which are known to be involved in plant immunity against microbial pathogens (Supplementary Data 1). Possibly, some of these NBS-LRR genes with upregulated expression in *TaSGR1*OE plants leaves contribute to defense responses against *Pst* infection.

To further characterize the role of *TaSGR1* in stripe rust resistance, CRISPR–Cas9-mediated gene editing was employed to fully inactivate three *TaSGR1* homoeologs in the wheat genome. Three genetically edited plants were obtained, containing nucleotide deletions leading to frameshift mutations in the region targeted by Cas9 in *TaSGR1-5A* and *TaSGR1-5B* (*tasgr1-AB*), in *TaSGR1-5B* (*tasgr1-B*), or in all three *TaSGR1* homoeologs (*tasgr1-ABD*), using three pairs of primers specific to the aforementioned three *TaSGR1* homoeologs (Supplementary Fig. 7a). After inoculation with the avirulent *Pst* CYR23, a typical resistance response with HR was observed in the inoculated Fielder plants, whereas the *tasgr1-ABD*, *tasgr1-AB*, and *tasgr1-B* plants developed evident urediniospore pustules (Fig. 1f, Supplementary Fig. 7b). Analysis of fungal biomass revealed increases of over 75%, 67%, and 56% in the *tasgr1-ABD, tasgr1-AB*, and *tasgr1-B* plants, respectively, compared to Fielder plants at 5 dpi (Fig. 1g, Supplementary Fig. 7c). Consistently, the transcription levels of *TaPR1* and *TaPR2* were reduced by over twofold at 24 and 48 hpi in *tasgr1-ABD* plants compared with those in Fielder plants (Fig. 1h). A Chl breakdown assay showed that the Chl content was slightly higher in the leaves of *tasgr1-ABD* plants than in those of Fielder plants (Fig. 1i). Additionally, hyphal length and infection areas were also greater at 24 and 48 hpi in *tasgr1-ABD* plants (Supplementary Fig. 7d, e). Based on these results, along with the demonstrated resistance conferred by TaSGR1 overexpression, *TaSGR1-5B* appears to contribute to plant resistance against *Pst*.

TaSGR1 physically associates with the thioredoxin TaTrx, a key factor for wheat resistance to *Pst*

To further explore the mechanism by which TaSGR1 influences the plant immune response, potential TaSGR1-interacting proteins were identified by screening a yeast two-hybrid (Y2H) library constructed with RNA isolated from *Pst*-infected wheat leaves. Twenty-three candidate binding proteins were identified, including eight chloroplast proteins and fifteen nonchloroplast proteins (Supplementary Data 3). Due to the localization of TaSGR1 in the chloroplasts, we focused on the eight chloroplast-related interactants and confirmed via Y2H assays that two of them, i.e., a known interacting protein (Chl a-b binding protein)[25] and a thioredoxin protein (TaTrx), interacted with TaSGR1 (Fig. 2a).

To corroborate these findings, the subcellular localization of TaTrx (TraesCS5A02G110300) in wheat protoplasts was first examined due to the lack of cTP. TaTrx-GFP localization was dependent on its N-terminal sequence for import into the chloroplasts, but its N-terminal sequence was uncleavable (Supplementary Fig. 8). The TaTrx–TaSGR1 interaction was further confirmed via bimolecular fluorescence complementation (BiFC) assay. In tobacco cells expressing TaSGR1-nEYFP and TaTrx-cEYFP, fluorescence signals of the TaSGR1–TaTrx interaction were specifically observed in the chloroplasts (Fig. 2b). Conversely, no fluorescence signals were detected in these organelles when the negative control TaSGR1$^{1-51}$-nEYFP and TaTrx-nEYFP were transiently expressed (Fig. 2b). Furthermore, co-immunoprecipitation (Co-IP) assays showed that TaSGR1-HA proteins strongly interacted with TaTrx-GFP but not with GFP alone, proving that TaSGR1 interacted with TaTrx in vivo (Fig. 2c). Moreover, the two haplotypes of TaSGR1-5B interacted with TaTrx in yeast (Supplementary Fig. 2d). To identify the TaSGR1-interacting region, prey constructs of TaSGR1 fragments containing the STAYGREEN domain at the N-terminal or the cysteine-rich region at the C-terminal were generated (Fig. 2d). TaTrx interacted with the STAYGREEN domain but not with the cysteine-rich region of TaSGR1 (Fig. 2d). These results suggest that TaSGR1 physically interacted with TaTrx in the chloroplasts.

To test the function of TaTrx in wheat during *Pst* infection, all three *TaTrx* homoeologs in the wheat genome were inactivated via CRISPR–Cas9 gene editing in Fielder plants, and one *tatrx-ABD* plant was obtained in which all three *TaTrx* homoeologs contained deletions leading to frameshift mutations in the targeted region (Supplementary Fig. 9a). A commercial anti-Trx antibody was used to detect the recombinant protein TaTrx-GST (Supplementary Fig. 9b). TaTrx protein was then detected via western blotting with anti-Trx antibody and the protein accumulation was substantially lower in *tatrx-ABD* plants than in Fielder (Supplementary Fig. 9c). Fielder plants inoculated with the avirulent *Pst* CYR23 showed strong HR with no pustules, whereas *tatrx-ABD* plants developed sporadic urediniospore pustules (Fig. 2e). The *tatrx-ABD* plants exhibited a 60% increase in the fungal biomass of CYR23 compared with Fielder plants (Fig. 2f). Additionally, a two- to threefold reduction in the expression of *TaPR1* and *TaPR2* was observed at 24 and 48 hpi in *tatrx-ABD* plants compared with Fielder plants (Supplementary Fig. 9d). These results confirmed that the loss of *TaTrx* dramatically impairs wheat resistance to *Pst*.

TaSGR1 is transformed from oligomer to monomer by TaTrx protein

When the structure of TaSGR1 was analyzed, a conserved cysteine-rich motif was predicted to possibly form disulfide bonds (Supplementary Fig. 2). To test whether TaSGR1 forms potential disulfide bonds dependent on the cysteine-rich motif, mutations were introduced into the TaSGR1 construct to alter the sequences encoding each of the five conserved cysteines (C241A, C245A, C247A, C248A, and C253A) without causing structural changes (Supplementary Fig. 10a). Y2H, BiFC, and Co-IP assays revealed that TaSGR1 still interacted with itself, but TaSGR1^{5A} (all five cysteines replaced by alanine) could not (Supplementary Fig. 10b–d). When these mutations were transiently expressed in *N. benthamiana*, three mutants (C247A, C248A, and C253A) showed more monomeric proteins than the wild-type TaSGR1, but TaSGR1^{5A} did not exhibit the oligomeric protein form (Fig. 3a). In vitro, the oligomerization of the recombinant protein TaSGR1-His was also observed on the gel; however, only monomeric TaSGR1-His was detected in vitro when the cross-links between proteins were cleaved by β-mercaptoethanol (β-ME) (Fig. 3b). These results confirm that TaSGR1 forms oligomers dependent on the cysteine-rich motif.

Studies have demonstrated that Trx proteins can reduce disulfide bridges in numerous target proteins[34,35]. Therefore, it was hypothesized that TaTrx may reduce the disulfide bonds in TaSGR1. To test this hypothesis, it was first determined whether the TaTrx protein exhibited disulfide reductase activity[36]. Insulin reduction assays were then performed, which revealed that TaTrx was able to accelerate the reduction of insulin in the presence of DTT, whereas GFP alone could not (Fig. 3c). TaTrxM, a mutation that replaced the conserved cysteines in the active site of redox-active disulfide bridges with an alanine, also failed to reduce insulin (Fig. 3c).

To confirm the effect of TaTrx on the oligomerization of TaSGR1, TaSGR1–TaTrx, and TaSGR1–TaTrxM were transiently co-expressed in *N. benthamiana*. In the presence of TaTrx, the abundance of TaSGR1 monomers increased, whereas that of TaSGR1 oligomers was reduced compared with leaves expressing TaSGR1–TaTrxM, in which the depolymerization of TaSGR1 was not detected (Supplementary Fig. 11a). These experiments were repeated in *TaSGR1*OE#1 and *TaSGR1*OE#3 transgenic wheat cells in which TaTrx and TaTrxM were highly expressed (Supplementary Fig. 12a), and the abundance of

https://doi.org/10.1038/s41467-025-58277-5

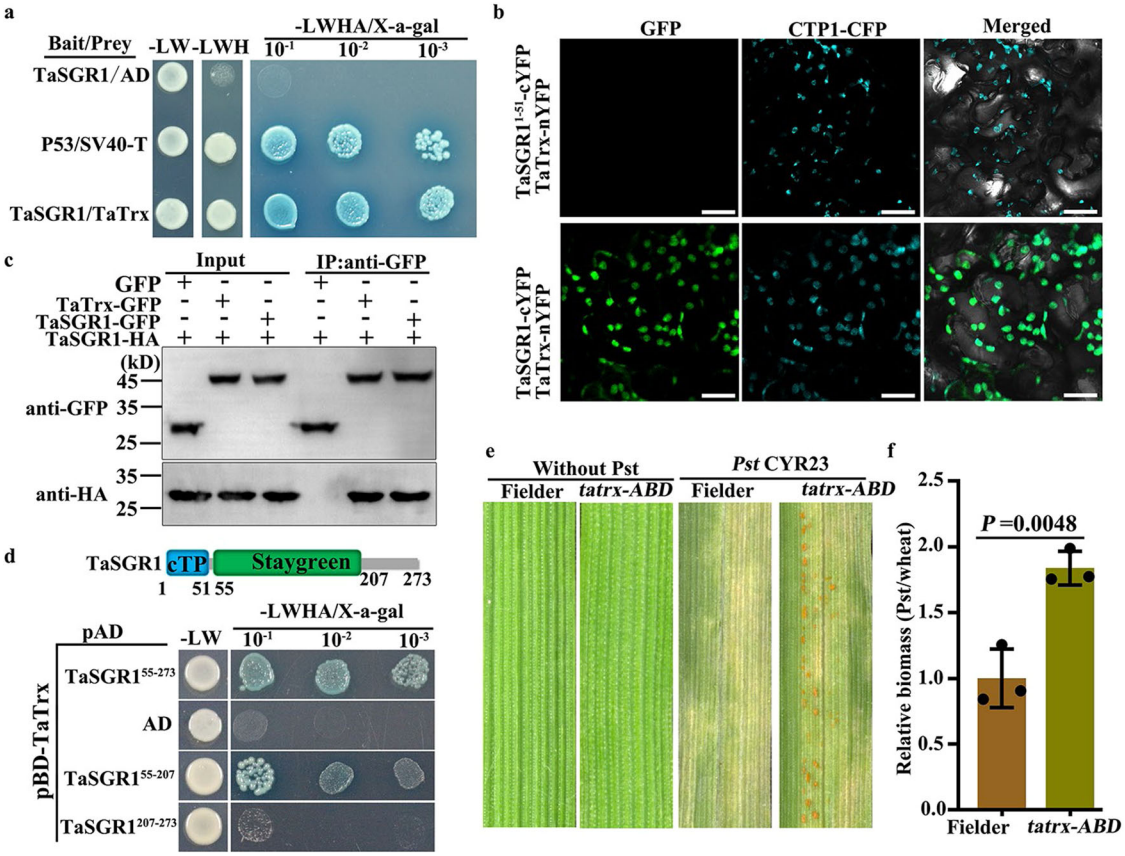

Fig. 2 | TaSGR1 interacts with the positive resistance regulator TaTrx. **a** Detection of the TaSGR1–TaTrx interaction via Y2H assays. P53/SV40-T and TaSGR1/AD were used as the positive and negative controls, respectively. **b** Interaction of TaSGR1 with TaTrx detected in the chloroplasts of *N. benthamiana* leaves transiently expressing the marked constructs via BiFC assays. TaSGR1$^{1-51}$, the cTP of TaSGR1; TaTrx$^{1-59}$. CTP1 fused with a CFP was used as a marker protein to localize into chloroplasts. Bar = 20 μm. **c** Confirmation of the TaSGR1–TaTrx interaction via Co-IP assays. Western blots of total proteins extracted from *N. benthamiana* leaves transiently expressing the marked constructs and proteins eluted from GFP-trap beads were detected using anti-GFP and anti-HA antibodies. **d** The STAYGREEN domain of TaSGR1 interacted with TaTrx in yeast cells. TaSGR1$^{55-207}$ contained the STAYGREEN domain. **e** Fielder and *tatrx* plants were inoculated with *Pst* CYR23, and disease phenotypes were observed at 14 dpi. **f** The *Pst*/wheat biomass in infected leaves was measured using qPCR. Means ± SD were determined based on three biological replicates from three leaf samples of different plants. The *P* value was determined using two-tailed unpaired Student's *t* test. Source data are provided as a Source Data file.

oligomeric TaSGR1 was reduced, whereas that of monomeric TaSGR1 was increased by the overexpression of TaTrx rather than TaTrxM (Fig. 3d). The detection of the TaTrxM–TaSGR1 interaction was performed to exclude the possibility that it might influence the depolymerization of TaSGR1. As observed for TaTrx, the TaTrxM mutation still interacted with TaSGR1 (Supplementary Fig. 11b). These results indicate that TaSGR1 is likely reduced from an oligomer to a monomer by TaTrx in plants.

TaSGR1 enhanced wheat resistance to *Pst* in a TaTrx-dependent manner

To evaluate whether rust infection affects the conformation of TaSGR1, it was detected in *TaSGR1*OE#L1 and #L3 plants treated with *Pst* CYR31. The results revealed the presence of monomeric and oligomeric TaSGR1 in *TaSGR1*OE plants that were not inoculated with *Pst* CYR31 (Fig. 3e). However, the levels of monomeric TaSGR1 were lower in *Pst*-inoculated *TaSGR1*OE plants than in noninoculated ones (Fig. 3e). In contrast, the levels of monomeric TaSGR1 were highe in *TaSGR1*OE plants inoculated with avirulent *Pst* CYR23 than in noninoculated ones (Supplementary Fig. 11c), indicating that TaSGR1 monomerization possibly contributes to plant resistance to *Pst*.

To determine whether monomeric TaSGR1 contributes to host resistance, we transiently expressed GFP, TaSGR1, and TaSGR1^{5A} in *tatrx* plants, followed by inoculation with *Pst* CYR34. Fourteen days post-*Pst* infection, *tatrx* plants expressing TaSGR1 produced fewer pustules compared with those expressing GFP (Fig. 4a). However, the introduction of TaSGR1^{5A} in *tatrx* plants resulted in a significant HR and a few urediniospore pustules (Fig. 4a). *tatrx* plants expressing TaSGR1 exhibited a 60% decrease in fungal biomass compared with those expressing GFP. However, leaves expressing TaSGR1^{5A} showed a 40% decrease in fungal biomass compared with those expressing TaSGR1 (Fig. 4b), indicating that TaSGR1 monomerization induced by TaTrx may contribute wheat resistance to *Pst*.

To further test that TaSGR1 monomerization promotes cell necrosis and leaf senescence, all the TaSGR1 mutations were transiently expressed in *N. benthamiana*. At 48 hpi, higher cell mortality and H_2O_2 accumulation were observed in leaves expressing TaSGR1^{5A} than in those expressing TaSGR1 alone or its mutations (Supplementary Fig. 13a, b). Additionally, detached leaves expressing TaSGR1^{5A} exhibited accelerated leaf yellowing compared with those expressing the other mutations (Supplementary Fig. 13c). Next, a semi-in vivo Chl degradation assay was conducted to evaluate the influence of TaTrx on TaSGR1 function. The results showed that TaSGR1 and each single mutation promoted Chl degradation, whereas TaSGR1^{5A} significantly accelerated Chl degradation compared with each single mutation (Fig. 4a). Additionally, the application of TaTrx enhanced the ability of

https://doi.org/10.1038/s41467-025-58277-5

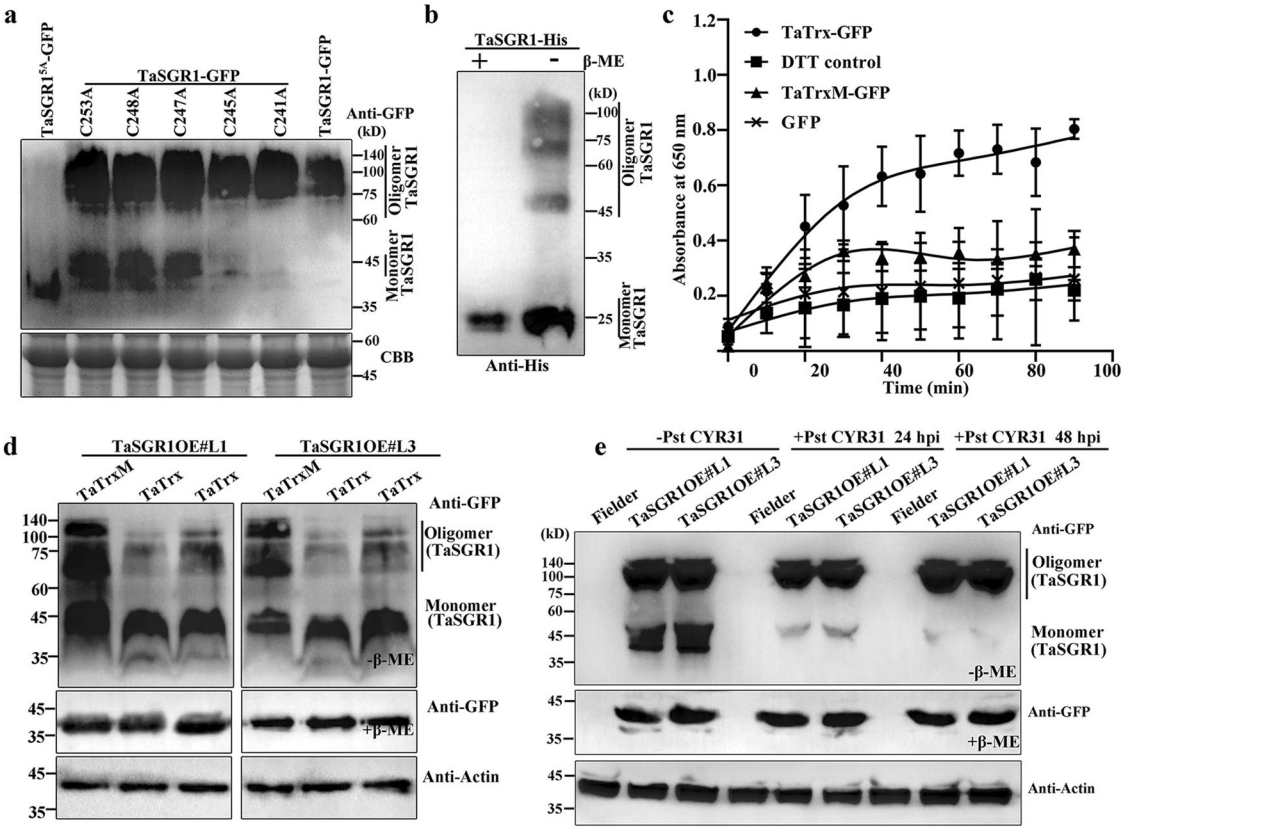

Fig. 3 | TaSGR1 is reduced from an oligomer to a monomer by TaTrx. a Cysteines at the C-terminal of TaSGR1 are essential for oligomerization. Total proteins extracted from *N. benthamiana* leaves transiently expressing TaSGR1-GFP, single mutations (C241A, C245A, C247A, C248A, and C253A), and TaSGR1^{5A}-GFP (all cysteines replaced by alanine) were detected using the anti-GFP antibody. **b** Detection of TaSGR1 oligomerization in vitro. TaSGR1-His purified from *E. coli* and treated with (+) or without (−) 5% β-mercaptoethanol (β-ME) was analyzed via immunoblotting using the anti-His antibody. **c** Measurement of the disulfide reductase activity of TaTrx using the turbidimetric assay of insulin reduction. Insulin reduction by DTT and GFP served as negative controls. TaTrxM is a mutant where two conserved cysteines in the active site of redox-active disulfide bridges were changed to alanine. Values are mean ± SD, $n = 3$ biologically independent samples. **d** The expression of *TaTrx* in *TaSGR1*OE#L1 and *TaSGR1*OE#L3 transgenic wheat lines promoted the transformation of TaSGR1 oligomers to monomers. Total proteins extracted from the leaves of *TaSGR1*OE#L1 and *TaSGR1*OE#L3 transgenic wheat plants transiently expressing TaTrx and TaTrxM were treated with or without β-ME and detected using the anti-GFP antibody. **e** The monomeric TaSGR1 were reduced in *Pst* CYR31-infected *TaSGR1*OE plants. Total proteins extracted from the leaves of *TaSGR1*OE plants were detected using the anti-GFP antibody. Actin proteins detected with the anti-Actin antibody indicated protein loading. Source data are provided as a Source Data file.

TaSGR1 to degrade Chl, whereas TaTrxM did not (Fig. 4b). To further confirm the influence of TaTrx on TaSGR1 function, TaSGR1–TaTrx and TaSGR1–TaTrxM were expressed in tobacco leaves. The cells co-expressing TaSGR1–TaTrx exhibited evidently higher H_2O_2 accumulation and electrolyte leakage but lower Chl content compared with those expressing TaSGR1 alone, whereas those co-expressing TaSGR1–TaTrxM and those expressing TaSGR1 alone exhibited similar Chl content, H_2O_2 accumulation, and electrolyte leakage (Supplementary Fig. 13d, e). These data suggest that TaSGR1 functions as a senescence-related factor to promote leaf senescence and H_2O_2 accumulation against *Pst* through its reduction from an oligomer to a monomer by TaTrx.

Pst_TTP1 is likely an intracellular effector targeting TaTrx

As tatrx plants showed increased susceptibility to avirulent *Pst* CYR23 upon infection, the function of TaTrx was examined to elucidate the underlying mechanism of redox regulation. To this end, attempts were made to identify candidate TaTrx interactors by screening a Y2H cDNA library generated from *Pst*-infected wheat leaves using TaTrx as bait, and Pst_TTP1 was identified as one of the interactors associated with TaTrx (Supplementary Data 4, Fig. 5a). Interestingly, BiFC assays in *N. benthamiana* showed that the fluorescence of the Pst_TTP1–TaTrx interaction was not concentrated in the chloroplasts (Supplementary Fig. 14a). This interaction was verified via Co-IP assays, and the results demonstrated that Pst_TTP1-HA proteins strongly interacted with TaTrx-GFP, whereas no significant binding was observed between Pst_TTP1-HA and TaSGR1-GFP or GFP alone (Fig. 5b).

To observe the diversity and intraspecies polymorphisms in Pst_TTP1, we compared its coding region among five different *Pst* isolates, including Chinese isolate CYR32, three US isolates (PST-21, PST-43, and PST-78), and one UK isolate (PST-87/7). Compared with the Pst_TTP1 sequence from CYR32, a total of 19 nucleotide substitutions were observed, including 10 synonymous substitutions and 9 nonsynonymous substitutions (Supplementary Fig. 15), indicating high levels of intraspecies polymorphism. Due to the lack of a stable transformation system, a Pst_TTP1NLS-GFP construct expressing a fusion of Pst_TTP1 and GFP with a nuclear localization sequence (NLS) was generated and transformed into another wheat pathogen, *Fusarium graminearum* PH-1, to determine whether Pst_TTP1 was delivered into wheat cells. GFP signals were observed in the nucleus of *F. graminearum*-infected wheat coleoptiles expressing the Pst_TTP1NLS-GFP construct, whereas no fluorescence signal was observed in coleoptiles where Pst_TTP1$^{\Delta SP}$NLS-GFP was expressed, indicating that Pst_TTP1 was indeed secreted and translocated into plant cells (Supplementary Fig. 14b).

https://doi.org/10.1038/s41467-025-58277-5

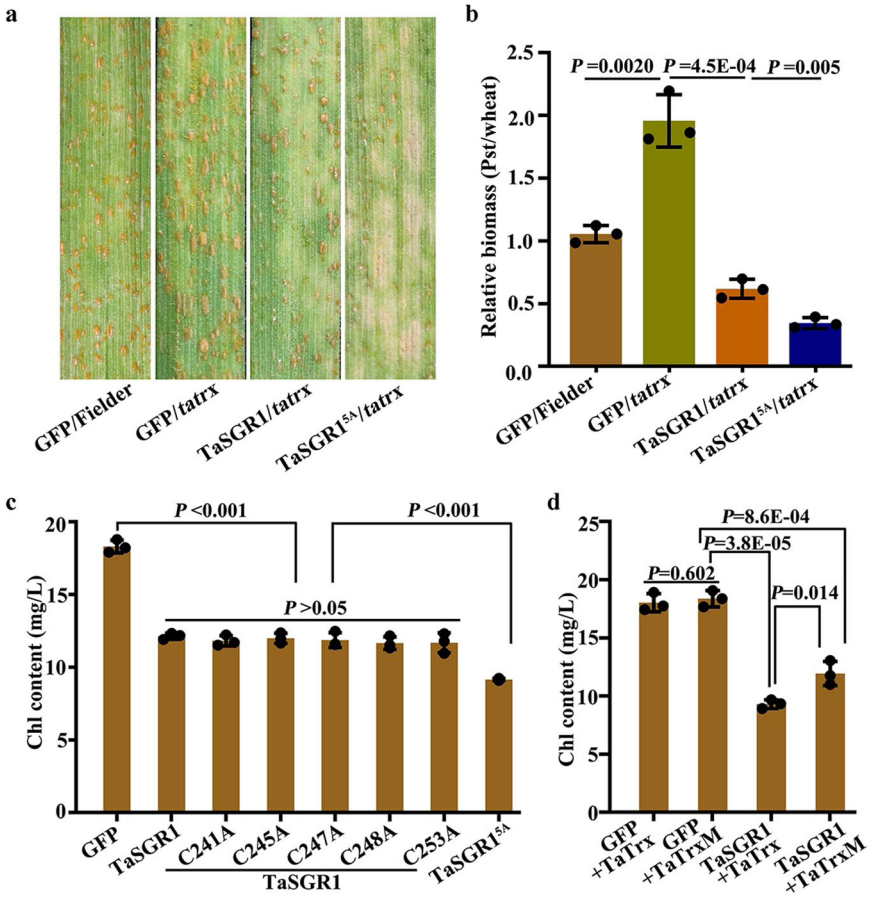

Fig. 4 | Monomeric TaSGR1 promotes plant resistance to *Pst*. **a** Monomeric TaSGR1 contributed to *Pst* resistance in wheat. TaSGR1^{5A} and TaSGR1 were transiently expressed in *tatrx* plants, respectively. Leaves were inoculated with *Pst* CYR31, and disease phenotypes were observed at 14 dpi. **b** The *Pst*/wheat biomass ratio reported in (**a**) was assayed using DNA isolated from the second leaves at 120 hpi. *TaEF1α* and *PstEF* were used to normalize the DNA levels of wheat leaves and *Pst*, respectively. **c** Semi-in vivo activity of TaSGR1 and its mutants. Spectrophotometric measurements of the Chl contents in crude Chl extract mixtures of *N. benthamiana* with the TaSGR1 protein were conducted as described in the methods. **d** TaTrx promoted Chl degradation by TaSGR1 in the semi-in vivo assay. Mixtures of equal amounts of TaTrx or TaTrxM and TaSGR1 were incubated with crude Chl extract, and Chl consumption was measured using a spectrophotometer. In (**b**–**d**), means ± SD were determined based on three biological replicates from three leaf samples of different plants. The *P* value was determined by two-tailed unpaired Student's *t* test. Source data are provided as a Source Data file.

Pst_TTP1 is required for the full virulence of *Pst*

The expression level of *Pst_TTP1* during *Pst*–wheat interaction was examined via qPCR. Compared with its level in urediniospores, Pst_TTP1 was highly induced, with its level increasing over 30-fold at 24 hpi (Supplementary Fig. 14c). To further determine the role of *Pst_TTP1* during wheat–*Pst* interaction, *Pst_TTP1* was knocked down via host-induced gene silencing, and two stable *Pst_TTP1*RNAi wheat lines were generated, i.e., P*st_TTP1*RNAi#L5 and #L7. Upon inoculation with *Pst* CYR31 and CYR34, these transgenic lines exhibited significant HR and few to no urediniospore pustules (Fig. 5c). The expression of *Pst_TTP1* in the two stable *Pst_TTP1*RNAi wheat lines was shown to decrease by 70–80% at 24 hpi (Fig. 5d). Compared with Fielder plants, *Pst_TTP1*RNAi wheat plants exhibited a 40–50% reduction in *Pst* biomass (Fig. 5e). Additionally, the measurement of H_2O_2 production in *Pst_TTP1*-knockdown wheat inoculated with *Pst* CYR31 revealed an increased accumulation of this peroxide at 24 and 48 hpi (Supplementary Fig. 14d, e). Collectively, these data indicate that P*st_TTP1* is required for the full virulence of *Pst* in wheat.

Pst_TTP1 prevents TaTrx from entering chloroplasts

Given that the fluorescence signals of the TaTrx–Pst_TTP1 interaction were observed in the cytoplasm, it was hypothesized that Pst_TTP1 suppressed TaTrx from entering the chloroplasts. With normal expression of the Pst_TTP1 protein, its subcellular localization was first confirmed in *N. benthamiana* and presented the same pattern as that of GFP alone (Supplementary Fig. 16a, b). Then, the interacting Pst_TTP1-HA and TaTrx-GFP were co-expressed in *N. benthamiana* to determine whether Pst_TTP1 affected the subcellular localization of TaTrx. An increase in GFP signals was detected in the cytoplasm of tobacco cells expressing Pst_TTP1-HA and TaTrx-GFP, whereas GFP signals were detected only in chloroplasts when TaTrx-GFP was transiently expressed alone (Supplementary Fig. 16c). These results were corroborated via chloroplast fractionation and immunoblotting. In the absence of Pst_TTP1, the TaTrx-GFP protein mainly accumulated in chloroplasts, whereas in the presence of Pst_TTP1, a large amount of TaTrx-GFP was detected in the cytoplasm (Supplementary Fig. 16d).

To test whether Pst_TTP1 prevented TaTrx from entering the chloroplasts in wheat leaves, Fielder plant leaves transiently expressing Pst_TTP1-HA-GFP or GFP alone were subjected to cell fractionation (Supplementary Fig. 12b). A small amount of TaTrx was detected in the cytoplasm of GFP (empty vector)-expressing leaves using the anti-Trx antibody (Fig. 6a). However, in leaves expressing Pst_TTP1-HA-GFP, the cytoplasm exhibited a strong accumulation of this protein (Fig. 6a). These results indicate that Pst_TTP1 prevented TaTrx from entering chloroplasts. To detect the translocation of TaTrx during *Pst*–wheat interaction, total chloroplast proteins were extracted from Fielder

https://doi.org/10.1038/s41467-025-58277-5

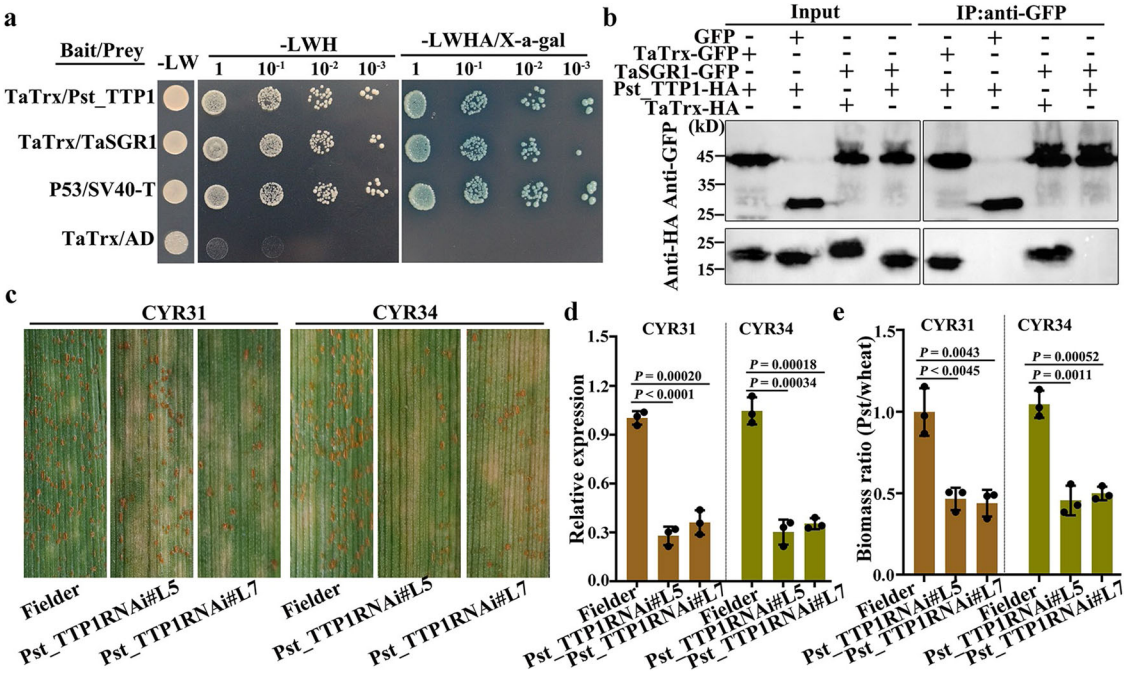

Fig. 5 | *Pst*-delivered Pst_TTP1 is required for the full virulence of *Pst*. **a** Detection of the Pst_TTP1–TaTrx interaction via Y2H assays. P53/SV40-T was used as the positive control. TaTrx/AD was used as the negative control. **b** Confirmation of the interaction between Pst_TTP1 and TaTrx in *N. benthamiana*. Total proteins extracted from *N. benthamiana* leaves transiently expressing the marked constructs were subjected to Co-IP assays and detected using the anti-GFP or anti-HA antibody. **c** The stable silencing of *Pst_TTP1* impairs *Pst* pathogenicity in transgenic wheat. Leaves were inoculated with *Pst* CYR31 and CYR34, and disease phenotypes were observed at 14 dpi. **d** Relative expression of *Pst_TTP1* in Fielder and *Pst_TTP1*RNAi plants inoculated with *Pst* CYR31 and CYR34 at 24 hpi. **e** The *Pst*/wheat biomass ratio reported in (**c**) was measured using DNA isolated from second leaves inoculated with *Pst* at 120 hpi. Wheat *TaEF1a* and rust *PstEF* were used to normalize the DNA level. In (**d** and **e**), means ± SD were determined based on three biological replicates. The *P* value was determined using a two-tailed unpaired Student's *t* test. Source data are provided as a Source Data file.

plants infected with *Pst* CYR34 or treated with ddH_2O. TaTrx was abundant in the chloroplasts in wheat leaves; however, it was also present in part in the cytoplasm at the early stage of *Pst* infection, which was not observed in noninfected control plants (Supplementary Fig. 16e).

To determine whether the chloroplast localization of TaTrx contributes to host resistance, TaTrx and $TaTrx^{60\text{-}175}$, and TaTrxM were transiently expressed in *tatrx* plants, which were then inoculated with *Pst* CYR23. *tatrx* plants expressing TaTrx showed strong HR with no pustules, whereas the control plants expressing $TaTrx^{60\text{-}175}$, TaTrxM, or GFP developed sporadic urediniospore pustules (Fig. 6b). These findings, which were further confirmed via fungal biomass assays (Fig. 6c), indicate that the presence of TaTrx in chloroplasts is required to confer resistance against *Pst* in wheat.

Pst-delivered Pst_TTP1 suppresses TaSGR1 function

To assess the effect of Pst_TTP1 on the conformation of TaSGR1, the following protein pairs were transiently expressed in *TaSGR1*OE wheat: Pst_TTP1 and GUS, TaTrx and GUS, and TaTrx and Pst_TTP1. Total proteins were then extracted from the plants and subjected to native PAGE without β-ME, followed by immunoblot analysis. The results showed that only oligomeric TaSGR1 was present in *TaSGR1*OE plants transiently expressing Pst_TTP1 (Fig. 6d). The amount of monomeric TaSGR1 in wheat cells expressing TaTrx and Pst_TTP1 was significantly lower than that in cells expressing TaTrx alone (Fig. 6d). Overall, these results suggest that Pst_TTP1 interacts with TaTrx and prevents it from entering chloroplasts, thereby suppressing the depolymerization of TaSGR1.

Subsequently, the influence of Pst_TTP1 on TaSGR1-induced ROS accumulation in chloroplasts was assessed in tobacco plants. The co-expression of *TaTrx* and *TaSGR1* was shown to gradually induce a high accumulation of ROS in chloroplasts, whereas no significant changes in the oxidized dichlorofluorescein (DCF) signal were observed in leaves expressing TaTrxM compared with control leaves co-expressing GUS and *TaSGR1* (Fig. 6e). Importantly, the co-expression of *Pst_TTP1* and *TaSGR1* decreased ROS production in the chloroplasts compared with the levels observed in the control (Fig. 6e). In repeated experiments, TaTrx significantly increased TaSGR1-induced ROS production, but TaTrxM did not exert the same effect; conversely, *Pst_TTP1* expression decreased ROS accumulation in chloroplasts (Supplementary Fig. 14f). Therefore, Pst_TTP1 may weaken the function of TaSGR1 and suppress plant immunity, possibly by interfering with the localization of TaTrx in chloroplasts.

Discussion

Chloroplasts are involved in plant productivity and serve as major sensors of the external environment, regulating the cellular response to biotic or abiotic stress[37,38]. Numerous studies of plant–pathogen interactions have shown that pathogen-secreted virulence factors target and modify chloroplast functions to promote plant disease, such as HopN1 and HopI1 of *P. syringae*[39,40]. In our study, Pst_TTP1 was confirmed to act as a blocker in the plant cytoplasm to prevent TaTrx from entering the chloroplasts. This mechanism of action is similar to that of other *Pst* effectors shown to target a chloroplast protein, TaISP[33,41]. TaTrx is a small thiol-disulfide oxidoreductase vital for the redox regulation of protein functions during plant development and stress responses[34,42]. In *Arabidopsis*, the deficiency of AtTRX m1, AtTRX m2, and AtTRX m4 disrupted the redox status of PSII core subunits, eventually leading to a pale-green leaf phenotype[43,44]. Although TaTrx is annotated as an m-type Trx, the inactivation of TaTrx in wheat did not result in the leaf chlorosis phenotype, possibly due to differences in the protein sequence between TaTrx and

https://doi.org/10.1038/s41467-025-58277-5

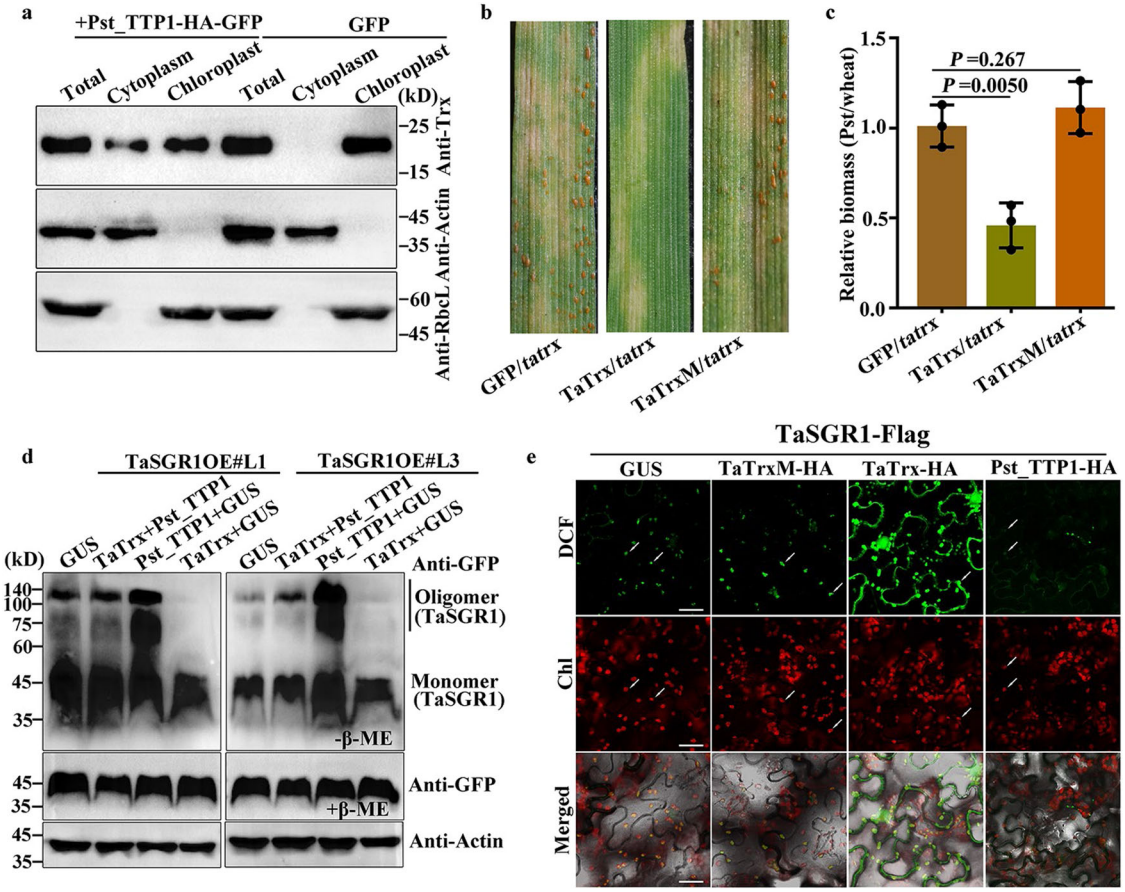

Fig. 6 | Pst_TTP1 prevents TaTrx from entering chloroplasts to induce wheat susceptibility to *Pst*. **a** Pst_TTP1 expression in Fielder plants using BSMV impaired the translocation of endogenous TaTrx to the chloroplast. Total proteins, cytoplasmic proteins, and chloroplast proteins were isolated and detected via immunoblotting with a specific anti-Trx antibody. Anti-Actin and anti-RbcL antibodies were used as markers for cytoplasmic and chloroplast proteins, respectively. **b** Transient overexpression of TaTrx, but not TaTrxM, promoted resistance to *Pst* in *tatrx* plants. TaTrx and TaTrxM were transiently expressed in the leaves using BSMV, followed by inoculation with *Pst* CYR23, and disease phenotypes were observed at 14 dpi. **c** The *Pst* biomass value reported in (**b**) was measured using qPCR. The *Pst*/wheat biomass ratio was determined using DNA isolated from the second leaves at 120 hpi. Means ± SD were obtained from three biological replicates from three leaf samples of different plants. The *P* value was determined using a two-tailed unpaired Student's *t* test. Source data are provided as a Source Data file. **d** *Pst_TTP1* expression in *TaSGR1*OE plants impaired the reduction of TaSGR1. *Pst_TTP1* and *TaTrx* were transiently expressed in *TaSGR1*OE plants using BSMV, and total proteins were extracted from the leaves and detected using the anti-GFP antibody. Actin was used as a loading control. Similar results are obtained from two independent biological experiments. **e** Effect of Pst_TTP1 and TaTrx on TaSGR1-induced ROS in chloroplasts. Tobacco leaves infiltrated with *Agrobacterium* expressing TaTrxM-HA–TaSGR1-Flag, TaTrx-HA–TaSGR1-Flag, Pst_TTP1-HA–TaSGR1-Flag and GUS–TaSGR1-Flag (control) and treated with H_2DCF-DA were observed to determine the presence of DCF signals. Arrows indicate the DCF signals in chloroplasts. DCF the oxidized dichlorofluorescein. Bar = 20 μm. Similar results are obtained from three independent biological experiments.

these m-type TRXs of *Arabidopsis*. Notably, unlike other AtTRX proteins, TaTrx might not possess any canonical import sequences or it carries uncleavable pre-sequences, which available prediction algorithms fail to recognize. Whether it may have other strategies to localize to chloroplasts such as with the help of other chloroplast proteins or be modified for import into the chloroplast is still unknown and would be an intriguing story to further investigate. The N-terminal sequence deletion of TaTrx failed to restore chloroplast localization and defense function, prompting us to speculate that the Pst_TTP1 effector hijacks TaTrx to suppress chloroplast functions and plant immunity. In recent years, increasing evidence has accumulated supporting a central role of thioredoxin in plant immunity through the regulation of redox signals and the fact that it is targeted by pathogen virulence factors, such as RipAY of *R. solanacearum* and victorin of *Cochliobolus victoriae*[45,46]. Additionally, the viral γb protein of barley stripe mosaic virus (BSMV) has been shown to interact directly with NbTRXh1 and suppress NbTRXh1 reductase activity to increase BSMV cell-to-cell movement[47]. Thus, these types of pathogens may directly attack the core components of thiol-dependent signaling in chloroplasts to establish a favorable environment for proliferation.

In terms of the biochemical properties of plants, the functions of Trx, including disulfide transferase, disulfide isomerase, disulfide reductase, and molecular chaperones, are believed to be among the most complex[35,44]. *Arabidopsis* Trx-f and Trx-m act as a key redox factor for the activation of photosynthetic enzymes in chloroplasts, such as fructose-1,6-bisphosphatase and NADP-malate dehydrogenase[44]. However, ZmTrxh of *Zea mays*, as a chaperone protein, disperses in the plant cytoplasm to suppress the accumulation of sugarcane mosaic virus RNA, which depends on chaperone activity instead of disulfide reductase[48]. In wheat, TaTrx exhibits disulfide oxidoreductase activity dependent on the conserved WC(G/P)PC motif with two active-site cysteines and acts as a disulfide reductase to catalyze the reduction of disulfide bonds in the TaSGR1 protein, possibly regulating protein structure, function, and monomerization, which can be interpreted in three ways. First, increase in the number of TaSGR1 monomers due to its depolymerization by TaTrx leads to the leaf chlorosis phenotype. Second, the monomers of TaSGR1 may enhance its ability to degrade

https://doi.org/10.1038/s41467-025-58277-5

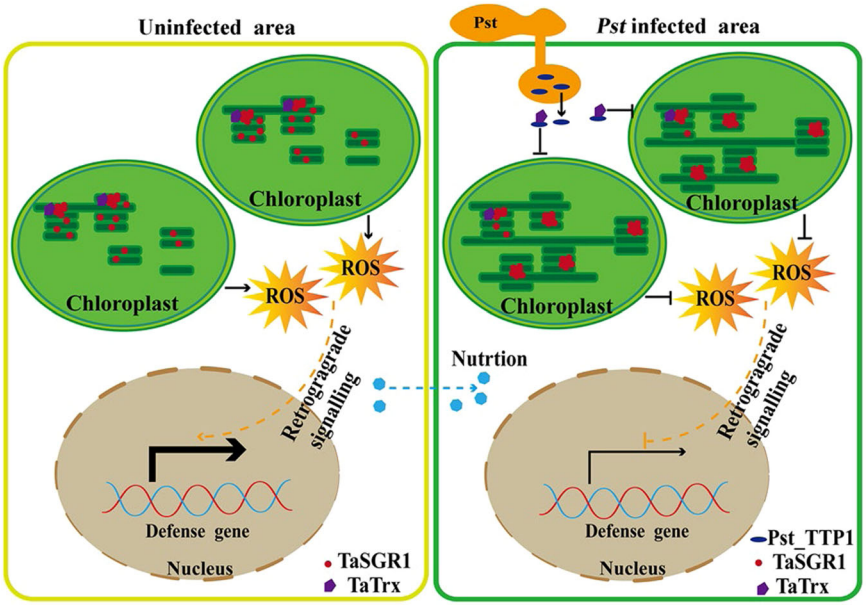

Fig. 7 | Working model of the role of the Pst_TTP1–TaTrx–TaSGR1 cascade during *Pst*–wheat interaction. In infected plant cells, the Pst_TTP1 effector is secreted and translocated into the plant cytoplasm, where it interacts with TaTrx, a plastidial thioredoxin, preventing its entry into chloroplasts. This disruption the transformation of TaSGR1 oligomers into monomers and attenuates the chlorophyllase activity of TaSGR1, leading to a reduced ROS accumulation and inhibition of the plant defense response. In neighboring uninfected cells lacking Pst_TTP1, TaTrx functions normally to regulate the TaSGR1 redox state within the chloroplasts, facilitating Chl recycling and the remobilization of nutrients, which may subsequently be transferred into the infected wheat cells. The green bars indicate stacked grana thylakoids in the chloroplast.

Chl. Third, TaTrx may also affect the structure of TaSGR1 to determine its function in Chl degradation. In *Arabidopsis*, Trx-h3 and Trx-h5 catalyze the transition of NPR1 oligomers to monomers to induce transcriptional reprogramming and disease resistance[49,50]. These findings suggest that redox signals are mediated by TaTrx during pathogen challenges, directly influencing the conformational changes of TaSGR1 to strengthen chloroplast-dependent plant immunity and improve wheat resistance to *Pst*.

STAY-GREEN (SGR) proteins play key roles in regulating plant chlorophyll degradation and senescence[25]. TaSGR1 knockout weakened the wheat immune response in Fielder plants, whereas its overexpression substantially enhanced resistance to multiple *Pst* isolates. Although Yr6 and Yr20 have been reported in Fielder plants[51], no studies have explored whether these genes, or other Yr gene confer plant resistance to *Pst* CYR23. We speculated that TaSGR1 is expressed the downstream of effector-triggered immunity (ETI) caused by the interaction between avirulent protein (Avr) and resistant (R) protein. TaTrx–TaSGR1 module acts as a plant immune component to regulate chlorophyll degradation and ROS accumulation in chloroplasts. Stable silencing of *Pst_TTP1* may release the TaTrx–TaSGR1 module, thereby drastically increasing ROS accumulation and cell death in Fielder plants. Therefore, we speculate that Pst_TTP1 acts as virulent secreted protein to suppress the function of TaTrx-TaSGR1 module and disrupt ETI. In addition, the high interspecies variation of Pst_TTP1 may be related to *Pst* virulence and overcoming plant defense responses. However, we cannot rule out the possibility that Pst_TTP1 can indirectly interact with R protein. It remains unknown whether Pst_TTP1 is an Avr protein, which can be confirmed by the corresponding R protein.

Several biotrophic fungi are known to establish close associations with their hosts by inducing the formation of green islands, which delay senescence and enable prolonged nutrient uptake[52,53]. This study identified a *Pst* effector, Pst_TTP1, that inhibits the plastidial TaTrx from entering the chloroplasts, thereby suppressing the redox signaling cascade to TaSGR1. The inability of TaTrx to depolymerize TaSGR1 delayed plant leaf senescence and reduces H_2O_2 accumulation, providing an explanation for the characteristic green islands observed at infection sites on wheat leaves (Fig. 7). These green islands likely redirect carbohydrate and nitrogen flows from neighboring aging cells into wheat cells within the infected green island areas[54]. Additionally, it has been reported that fungal hyphae proliferating vigorously at infected sites create a strong nutrient sink, mobilizing resources from uninfected cells[53]. This process considerably enhances the efficiency of rust fungi in nutrient acquisition for reproduction.

Increasing plant yield and disease resistance are two major goals for breeding. Crops are usually bred to maximize growth-related traits, which could inadvertently lead to the loss of useful genetic traits for defense[55]. There are few reports of a single gene positively regulating both yield and resistance. IPA1 in rice is a good example[56]. Our study suggests that overexpression of TaSGR1 leads to leaf chlorosis and a significant decrease in photosynthetic efficiency and wheat yield, whereas ROS accumulation and the transcript levels of defense-related genes are obviously higher, indicating that TaSGR1 probably participates in the fine-tuning between disease resistance and growth and development. Thus, balancing growth and plant defense will be crucial for future crop breeding strategies aimed at developing superior crop varieties that combine high yields with robust resistance to biotic stressors. Although loss-of-function mutations in MLO or RBL1 result in broad-spectrum resistance, this is also accompanied by substantial growth and yield penalties[57,58]. However, the application of sophisticated genome-editing technologies breaks the growth–immunity trade-off by promoting both disease resistance and yield[57,58]. Whether controlled or conditional expression of TaSGR1 offers a more fine-tuned and moderate immune activation without growth defects would be an intriguing topic for further investigation. This work shows that the TaTrx–TaSGR1 cascade mediates plant defense and growth and development, offering valuable targets for breeding crop varieties with efficient disease resistance and high yield.

Methods

Experimental materials and growth conditions

The wheat cultivar Fielder was used to create transgenic wheat lines including *TaSGR1* overexpression (*TaSGR1*OE) lines, *TaSGR1* knockout (*tasgr1-ABD*) lines, *TaTrx* knockout (*tatrx*) lines, and *Pst_TTP1*RNAi lines. For tillering and seed collection, Fielder and other transgenic plants were grown in Pindstrup soil (Pindstrup Mosebrug A/S) at 25 °C with 16 h of light and 20 °C with 8 h of dark. For *Pst* inoculation, all plants were grown in a greenhouse under 8/16 h night/day conditions at 16 °C and inoculated on the second leaves of two-leaf stage wheat. *N. benthamiana* was grown on Pindstrup soil in a greenhouse at 23 °C under 16 h light/8 h dark for transient expression assays. Chinese *Pst* isolates CYR23, CYR31, and CYR34 were obtained from the culture collection of the State Key Laboratory (Northwest A&F University). For propagation, the *Pst* CYR23 was inoculated on wheat cultivar MX169, and CYR31 and CYR34 were grown on the second leaves of two-leaf stage wheat cultivar Suwon 11 at 16 °C as previously described[59]. Briefly, 0.05 mg of fresh urediniospores was suspended in 2 mL of water and then used to inoculate wheat leaves at the two-leaf stage using a fine paintbrush. After inoculation, wheat seedlings were kept in a humid chamber for 24 h at 16 °C and then returned to the growth chamber at 16 °C. At 14 dpi, fresh *Pst* urediniospores were collected and stored at 4 °C.

Transgenic wheat and constructs

For the RNAi construct, the specific fragment of *Pst_TTP1* (172 bp) was amplified using the full-length *Pst_TTP1* as a template with specific primer pairs listed in Supplementary Data 5. All PCR assays were performed under the following conditions: preheating at 95 °C for 30 s, followed by 40 cycles (95 °C for 10 s, 55–60 °C for 30 s, 72 °C for 10–60 s), and a final extension at 72 °C for 10 min. The amplified product was inserted into the RNAi vector pLGY-OE3 in both antisense and sense orientations behind the Ubi promoter using a highly efficient DNA seamless cloning kit (Vazyme, C112-01). For constructing the TaSGR1 overexpression vector, the full-length coding sequence of TaSGR1 was amplified and inserted into the pCAMBIA1302 vector using a highly efficient DNA seamless cloning kit (Vazyme, C112-01). For editing TaSGR1 and TaTrx with CRISPR–Cas9, two candidate guide RNAs (gRNAs) targeting the three copies of TaSGR1 and TaTrx were designed and are shown in Supplementary Data 5, and their editing efficiencies were determined using WheatOmics (http://202.194.139.32/). These gRNAs exhibiting high efficiency were introduced into the pBUE411 vector to create the CRISPR–Cas9 vector[60]. The resulting constructs were transformed into *A. tumefaciens* strain EHA105. The transgenic wheat lines were generated through *Agrobacterium*-mediated infiltration of immature embryos of the wheat cultivar Fielder as described above[61]. The positive transgenic seedlings were selected with BASTA (100 mg/L), and genomic DNA from transgenic wheat lines was extracted for PCR detection of the Cas9 gene fragment.

Gene overexpression mediated by BSMV

To induce the expression of TaTrx, TaTrxM, TaSGR1, or TaSGR1^{5A} in wheat leaves, the corresponding full-length genes were amplified via PCR from wheat cDNA and inserted into the BSMV-VOX vector (γ vector) using a highly efficient DNA seamless cloning kit (Vazyme, C112-01) according to the manufacturer's instructions[62]. One microgram of the corresponding recombinant vectors was linearized using the *MluI* restriction enzyme (New England Biolabs, R3198V), and 1.0 μg of linearized DNA was transcribed to RNA in vitro using the RiboMAX large-scale RNA production system T7 (Promega, P1300). The transcripts of each vector (α, β, γ, or recombinant γ-gene) were mixed in a 1:1:1 ratio as previously described[62] and then inoculated onto the second leaves of two-leaf-stage wheat plants by gently rubbing (3–5 times) the surface with a gloved finger. The BSMV-infected plants were grown under a relative humidity of 90% in darkness for 24 h at 26 °C. At 10 dpi, total proteins were extracted from the wheat leaves expressing the corresponding vectors, and *Pst* was inoculated on the fourth leaves. At 14 dpi with *Pst*, 20–30 infected leaves were sampled for phenotype identification.

Y2H assay

The full-length coding sequences of *TaSGR1*, *Pst_TTP1*, and *TaTrx* were amplified using cDNA from *Pst*-infected wheat as a template with the specific primer pairs listed in Supplementary Data 5. All PCR assays were performed under the following conditions: preheating at 95 °C for 30 s, followed by 40 cycles (95 °C for 10 s, 55–60°C for 30 s, 72 °C for 10–60 s), and a final extension at 72 °C for 10 min. The amplified product was inserted into the vector pGBKT7 or pGADT7 using a highly efficient DNA seamless cloning kit (Vazyme, C112-01). A binding domain fusion of TaSGR1 (pGBKT7-TaSGR1) or TaTrx (pGBKT7-TaTrx) was used to screen a cDNA library following the Y2H system protocol (CLONTECH Laboratories). The cDNA library was constructed from *Pst* CYR32-infected wheat cultivar Avocet at 24 hpi. One microgram of pGBKT7-TaSGR1 and pGADT7-TaTrx, or pGBKT7-TaTrx and pGADT7-Pst_TTP1, were co-transformed into the yeast strain AH109 following the Y2H system protocol (CLONTECH Laboratories) as previously described[33]. We performed the Y2H assay for all eight candidates with TaSGR1, and a single clone was cultured in liquid medium (SD/-Leu/-Trp) at 30 °C and 200 rpm for 24 h. Then, yeast cells were suspended in sterile water at OD_{600} = 0.5 and diluted onto the corresponding medium (SD/-Leu/-Trp/-His and SD/-Leu/-Trp/-His/-Ade) for the selection of transformants.

BiFC and subcellular localization

For the BiFC assay in *N. benthamiana* leaves, the full-length coding sequences of TaSGR1 and Pst_TTP1 (without the signal peptide) were ligated with YFP in the vector pSATN-nEYFP, and TaTrx was cloned into pSATN-cEYFP. The constructs were transformed into *A. tumefaciens*. *Agrobacterium*-transformed cells containing TaSGR1-nYFP and TaTrx-cYFP, TaTrx-cYFP and Pst_TTP1-nYFP were mixed at OD_{600} = 0.6. After 48 h of infiltration, images were captured by confocal microscopy with a 488-nm laser. For subcellular localization in *N. benthamiana*, TaTrx and Pst_TTP1 were cloned into the pCAMBIA1302 vector with a GFP tag and transformed into *A. tumefaciens* GV3101. *Agrobacterium* was infiltrated into *N. benthamiana* leaves at OD_{600} = 0.6, and images were captured using confocal microscopy with a 488-nm laser after 48 h of infiltration. For subcellular localization in wheat protoplasts, TaSGR1 and TaTrx were cloned into the pJIT163-hGFP vector and transformed into wheat protoplasts using PEG-mediated transformation as previously described[63]. GFP signals were observed and photographed using confocal microscopy (Leica STELLARIS STED/EM CPD300) (ocular: 10×; objective: 10×) under laser excitation at 488 nm and emission at 512–527 nm. Cyan fluorescent protein (CFP) signals were observed under laser excitation at 405 nm and emission at 485 nm. Chl fluorescence was captured under an excitation wavelength of 490 nm and emission wavelength of 650–750 nm.

Co-IP assay

For the Co-IP assay in *N. benthamiana*, the coding sequences of TaTrx and Pst_TTP1 were cloned into the expression vector pICH86988 (HA tag), and the interacting genes were cloned into the pCAMBIA1302 vector (GFP tag). *A. tumefaciens* cells containing the various constructs were collected and diluted to OD_{600} = 0.6 and then infiltrated into the leaves of 4-week-old *N. benthamiana*. After 48 h, total proteins were extracted using extraction buffer (25 mM Tris-HCl [pH 7.5], 1 mM EDTA, 150 mM NaCl, 2% polyvinylpolypyrrolidone, 10% glycerol, 10 mM DTT, 1× protease inhibitor, and 1 mM PMSF). Following centrifugation (15,000 × *g* for 15 min at 4 °C), the supernatant was incubated at 4 °C for 2 h in the presence of GFP-trap agarose (Chromotek, gta-20). The beads were collected and washed three times with 500 μL

of extraction buffer. Proteins bound to the agarose beads were boiled in protein sample loading buffer for 10 min and detected via western blotting. For immunodetection, the corresponding proteins on the PVDF membrane were detected using an anti-GFP antibody (Beyotime, AF0159, 1:5000) or an anti-HA antibody (Beyotime, AF2858, 1:5000), with a secondary goat anti-mouse IgG-peroxidase-conjugate antibody (Beyotime, A0192, 1:2000).

Assays for the localization of Pst_TTP1 during plant infection

To assess the secretion of Pst_TTP1 in wheat, the Pst_TTP1-GFP-NLS fusion sequence (amino acid sequence: PKKKRKV) was generated via overlapping PCR, incorporating the NLS from the simian virus large T antigen. The amplified product was inserted into the pFL2 vector using a highly efficient DNA seamless cloning kit (Vazyme, C112-01) according to the manufacturer's instructions. The recombinant vector was then transformed into *A.tumefaciens* and co-cultured with *F. graminearum* strain PH-1 to obtain transformants as previously described[64]. Conidia of *F. graminearum* transformants were obtained from liquid carboxymethyl cellulose (CMC) medium incubated in a shaker at 200 rpm for 5 days and resuspended at a concentration of 10^5 spores/mL in sterile distilled water. About 5 µL of the conidial suspension was inoculated onto wheat coleoptiles of 3-day-old seedlings of cultivar SM126 as previously described[62]. GFP signals in the wheat coleoptiles were examined at 48 hpi using a confocal microscope equipped with a 488-nm laser.

Measurement of oxidative bursts and electrolyte leakage

ROS bursts were measured based on previously described protocols[65]. Leaf disks with a size of 0.5 cm^2 obtained from *N. benthamiana* transiently expressing *TaSGR1* and its mutations were placed overnight into a white 96-well plate containing 200 µL of water to eliminate damage-induced ROS. These leaf samples were subsequently treated with 200 µL of solution containing horseradish peroxidase at a concentration of 20 mg/mL and 100 mM luminol. Luminescence was measured using a multiscan spectrum for 60 min. Data were analyzed by plotting the total luminescence units detected during 60 min. Ion leakage from detached leaves was measured as previously described[65]. Six *N. benthamiana* leaf disks with a diameter of 1 cm were cut from leaves harvested 2 days after agroinfiltration and these disks were left floating on 5 mL of distilled water for 5 h with continuous shaking at room temperature. The initial electrolyte leakage values were measured using a conductivity meter (DDS-307; LEICI). Total conductivity was determined after incubating the samples at 100 °C for 20 min. The relative electrolyte leakage was calculated by comparing the initial and total conductivity values.

Histochemical analysis of *Pst*-infected wheat samples

To assess the cellular response of *Pst*-infected wheat, infected leaf samples were treated with DAB buffer (1.0 mg·mL^{-1}) under light conditions for 8 h. After treatment, the samples were decolorized in destaining buffer (absolute ethyl alcohol:acetic acid, 1:1 (v/v)) and then immersed in chloral hydrate. The samples were observed under an Olympus BX−51 microscope, and the area containing H_2O_2 was determined using the CellSens Entry software. To monitor *Pst* progression in wheat plants, infected leaves were collected at 24 and 48 hpi and cleaned with ethanol as described above[59]. The samples were then autoclaved in 2 mL of 1 M KOH at 121 °C for 5–6 min. After being washed three times with 50 mM Tris-HCl (pH 7.4), the rinsed fragments were subsequently incubated in wheat germ agglutinin solution. The *Pst* hyphal length and infection areas were observed using an Olympus BX−51 microscope, and measurements were made using CellSens Entry (version: V1.7). For each wheat leaf sample in each biological replication, 30 infection sites from three leaves of different plants were examined to record ROS accumulation, *Pst* hyphal length, and infection areas. The experiments were conducted in a completely randomized block design with three replications.

Extraction of genomic DNA and RNA and expression analysis

Genomic DNA was extracted from wheat leaves using the CTAB method for molecular detection. DNA from the *Pst*-inoculated leaves was extracted at 120 hpi for the analysis of fungal biomass. The relative biomass of rust fungal DNA was measured using the cycle threshold value (Ct) of the DNA elongation factor for *Pst* (*PstEF1*) against the Ct of the DNA elongation factor (*TaEF1a*) for wheat. All experiments were conducted in triplicate. Total RNA was extracted using a kit (Takara Bio Inc.) for plant RNA extraction following the manufacturer's instructions. A total of 1.5 µg RNA was used to synthesize first-strand cDNA using the PrimeScript reverse transcriptase (Takara Bio Inc.). Specific primer pairs (Supplementary Data 5) were designed, and *TaEF1a* (accession number: Q03033) and *PstEF1* (accession number: KNE93481) were selected as the internal control genes. qPCR amplifications were performed in a 20-µL reaction mixture containing 10 µL of ChamQ Universal SYBR qPCR Master Mix (Vazyme, Q711-02), 10 pmol each of the forward and reverse gene-specific primers, and 2 µL of diluted cDNA (1:10). All qPCR amplifications were performed on a CFX Connect Real-time instrument (Bio-Rad, USA) with the following conditions: preheating at 95 °C for 30 s, followed by 40 cycles at 95 °C for 10 s, 60°C for 30 s to assess the cycle threshold, and melt curves were obtained at 95 °C for 15 s, 60 °C for 1 min, and 95 °C for 15 s. Each qPCR amplification was repeated three biological replicates from three leaf samples of different plants. For detection of the expression pattern of *TaSGR1*, the control for qPCR was Fielder plants treated with water. For detection of the expression of defense-related genes in transgenic wheat, the control for qPCR was Fielder plants treated with *Pst*. Data were analyzed using the $2^{-\Delta\Delta CT}$ method. Statistical significance was determined based on the unpaired two-tailed Student's t test. All primers are shown in Supplementary Data 5.

RNA-seq analysis

The second leaves of two-leaf-stage wheat infected by *Pst* CYR34 were collected at 24 hpi and immediately frozen in liquid nitrogen for RNA-seq analysis. Three biological replicates were performed for each sample. RNA sequencing was conducted at the JMDNA Bio-Medical Technology Company using the Illumina Hiseq platform (JMDNA Bio-Medical Technology Co., Ltd., Shanghai). For data analysis, the processed reads were mapped to the reference genome of Chinese Spring (Accession: GCA_018294505) via Hisat2 (v2.0.1)[66]. DEGs were defined as transcripts with a fold change in expression level (according to FPKM value) >2.0 and a q-value < 0.05. Heatmaps of specific genes were generated using the pheatmap package of R. GO enrichment analysis was performed with the clusterProfiler package of R, and the enrichment criteria included a q-value < 0.05.

Chloroplast isolation and pigment analysis

Chloroplast isolation was performed based on previously described protocols[67]. In brief, 2 g of wheat leaves or *N. benthamiana* leaves were harvested and crushed into small pieces in a mortar. The samples were then ground to a paste with 1 mL of cold separation solution (0.35 M NaCl). The suspension was filtered into a 10-mL tube through a triple gauze pad, and the liquid was centrifuged at 1000 ×g for 5 min at 4 °C. Then, 100 µL of the supernatant and the sediment were added to 25 µL of 5× loading buffer, boiled for 10 min, and detected by western blotting. Actin proteins, detected with an anti-actin antibody (Abbkine, ABM40122), indicated cytoplasm protein loading, whereas the RuBisCO large subunit (RbcL), detected with an anti-RbcL antibody (Sangon Biotech, D191102-0050), indicated chloroplast protein loading. Wheat Trx protein was detected with a specific anti-Trx antibody (PhytoAB, PHY3066S). For pigment analysis, 200 mg of wheat and *N. benthamiana* leaves were cut and immediately immersed in 5 mL of

acetone and incubated at 4 °C in the dark for 12 h. Aliquots of total Chl dissolved in acetone were mixed with hexane and 10 mM KOH at a ratio of 4:6:1 (v/v), and the mixture was vortexed and centrifuged at 12,000 ×*g* for 10 min for phase separation. For semi-in vivo TaSGR1 activity[68,69], the corresponding proteins (i.e., TaSGR1-GFP, TaTrx-GFP) were expressed in *N. benthamiana* leaves and purified using GFP-trap agarose (Chromotek, gta-20) according to the above immunoprecipitation method. The purified fusion proteins were quantified using a Bradford protein assay kit (Beyotime, P0006) according to the manufacturer's instructions. 0.1-mL aliquots of the purified TaSGR1-GFP fusion (approximately 2 μg) were mixed with 0.1 mL of 0.1 M MOPS buffer (pH 7.0) and 0.2 mL of crude Chl extract. The mixture was incubated at 25 °C for 1 h, and the reaction was stopped by transferring 0.4 mL of the reaction mixture to tubes containing 0.4 mL of acetone plus 0.4 mL of hexane. The mixture was then vortexed and centrifuged at 12,000 ×*g* for 10 min to partition the remaining Chl into the hexane phase. The total Chl in the hexane phase was quantified using a multiscan spectrum at absorbances of 663 nm and 645 nm according to the following formula[70]: Total Chl in mg/L = $8.02A_{663} + 20.21A_{645}$.

Thioredoxin activity assay

The activity of TaTrx was assessed using the insulin reduction assay as previously described[36]. In brief, 5 mg of insulin was suspended in 4 mL of 0.05 M Tris-Cl (pH 7.4), adjusted to 5 mL with water, and stored at −20 °C. The assay mixture was prepared in a 96-well plate by adding 100 μL of insulin plus TaTrx-GFP (approximately 2 μg), TaTrxM-GFP, or GFP to obtain a final volume of 200 μL. TaTrx-GFP, TaTrxM-GFP, and GFP were expressed in *N. benthamiana* leaves and purified using GFP-trap agarose beads. The reaction was initiated by pipetting dithiothreitol (2–10 μL) into each well, excluding the blank. The contents were thoroughly mixed, and the plate was then placed in a spectrophotometer set to 650 nm. Six independent biological replicates were performed.

Chl fluorescence imaging

Chl fluorescence imaging of *N. benthamiana* and wheat was performed with a Chl fluorescence imager (Technologica Ltd.) according to the manufacturer's instructions described previously[7]. The wheat leaves of *TaSGR1*OE plants and 4-week-old tobacco leaves treated with *A. tumefaciens* GV3101 harboring the corresponding constructs were placed in the chamber for 24 h and then dark-adapted for 30 min. These leaves were then exposed to 5000 μmol m^{-2} s^{-1} for 0.8 s to obtain maximum dark-adapted fluorescence (Fm). Minimal fluorescence (Fo) and maximal fluorescence (Fm) were monitored using a very weak light (0.04 μmol m^{-2} s^{-1}) and a transient saturated light pulse (5000 μmol m^{-2} s^{-1}). Fv/Fm was calculated as (Fm − Fo)/Fm. Actinic light (120 μmol m^{-2} s^{-1}— the same as the plant growth light intensity) was then applied for 15 min, followed by a saturating pulse to obtain maximum light-adapted fluorescence (Fm´), and minimal fluorescence (Fo´) was measured after turning off the actinic light. NPQ was calculated as 1 − (Fm´ − Fo´)/(Fm − Fo).

Statistics and reproducibility

Image Lab (version 4.0) build 16 was used for DNA electrophoresis and WB data collection. All confocal micrographs were collected by Leica LAS X Hardware Configurator Version 2020.6.0. The related genes expression analysis of wheat samples infected with *Pst* were obtained from the transcriptome data (http://www.wheat-expression.com/). Their sequences were obtained from the Ensembl plant database (http://plants.ensembl.org/index.html), and sequence alignment was carried out using the online platform at http://multalin.toulouse.inra.fr/multalin/multalin.html. All data analysis was performed using GraphPad 8.0 and are shown as means ± standard deviation. The statistical analyses were performed using SPSS 26.0. The significant differences between experimental and control groups were determined by the two-tailed Student's t test, one way ANOVA. All experiments in this study were performed two to three times with similar results. No data were excluded from the analyses. The investigators were not blinded to allocation during experiments and outcome assessment.

Reporting summary

Further information on research design is available in the Nature Portfolio Reporting Summary linked to this article.

Data availability

GenBank accession codes include TraesCS5B02G320200 for *TaSGR1* genes, TraesCS5A02G110300 for *TaTrx* genes, XP_047799543 for *Pst_TTP1* genes (https://www.ncbi.nlm.nih.gov/). RNA-Seq data for *TaSGR1*OE plants and Fielder inoculated with *Pst* have been deposited in the NCBI Sequence Read Archive (SRA) under accession number PRJNA1186393. Data supporting the findings of this work are provided with this paper, Supplementary Information files, and repository platform. Source data are provided with this paper.

References

1. Savary, S. & Willocquet, L. Modeling the impact of crop diseases on global food security. *Annu. Rev. Phytopathol.* **58**, 313–341 (2020).
2. Miller, S. A., Beed, F. D. & Harmon, C. L. Plant disease diagnostic capabilities and networks. *Annu. Rev. Phytopathol.* **47**, 15–38 (2009).
3. Yi, M. & Valent, B. Communication between filamentous pathogens and plants at the biotrophic interface. *Annu. Rev. Phytopathol.* **51**, 587–611 (2013).
4. McCombe Carl, L., Greenwood Julian, R., Solomon Peter, S. & Williams Simon, J. Molecular plant immunity against biotrophic, hemibiotrophic, and necrotrophic fungi. *Essays Biochem.* **66**, 581–593 (2022).
5. Kamoun, S. A catalogue of the effector secretome of plant pathogenic Oomycetes. *Annu. Rev. Phytopathol.* **44**, 41–60 (2006).
6. Rafiqi, M., Ellis, J. G., Ludowici, V. A., Hardham, A. R. & Dodds, P. N. Challenges and progress towards understanding the role of effectors in plant–fungal interactions. *Curr. Opin. Plant Biol.* **15**, 477–482 (2012).
7. de Torres Zabala, M. et al. Chloroplasts play a central role in plant defence and are targeted by pathogen effectors. *Nat. Plants* **1**, nplants201574 (2015).
8. Hu, Y. et al. Bacterial effectors manipulate plant abscisic acid signaling for creation of an aqueous apoplast. *Cell Host Microbe* **30**, 518–529.e516 (2022).
9. Xian, L. et al. A Bacterial effector protein hijacks plant metabolism to support pathogen nutrition. *Cell Host Microbe* **28**, 548–557.e547 (2020).
10. Walters, D. R., McRoberts, N. & Fitt, B. D. L. Are green islands red herrings? Significance of green islands in plant interactions with pathogens and pests. *Biol. Rev.* **83**, 79–102 (2008).
11. Naseem, M., Wölfling, M. & Dandekar, T. Cytokinins for immunity beyond growth, galls and green islands. *Trends Plant Sci.* **19**, 481–484 (2014).
12. Avila-Ospina, L., Moison, M., Yoshimoto, K. & Masclaux-Daubresse, C. Autophagy, plant senescence, and nutrient recycling. *J. Exp. Bot.* **65**, 3799–3811 (2014).
13. Hörtensteiner, S. Chlorophyll degradation during senescence. *Annu. Rev. Plant Biol.* **57**, 55–77 (2006).
14. Fradin, E. F. & Thomma, B. P. H. J. Physiology and molecular aspects of Verticillium wilt diseases caused by *V. dahliae* and *V. albo-atrum*. *Mol. Plant Pathol.* **7**, 71–86 (2006).
15. Hovmøller, M. S., Walter, S. & Justesen, A. F. Escalating threat of wheat rusts. *Science* **329**, 369–369 (2010).
16. Dickman, M. B. & de Figueiredo, P. Death be not proud—cell death control in plant fungal interactions. *PLoS Pathog.* **9**, e1003542 (2013).

17. Kourelis, J. & van der Hoorn, R. A. L. Defended to the Nines: 25 Years of resistance gene cloning identifies nine mechanisms for R protein function. *Plant Cell* **30**, 285–299 (2018).
18. Wang, S. et al. YR36/WKS1-mediated phosphorylation of PsbO, an extrinsic member of Photosystem II, inhibits photosynthesis and confers stripe rust resistance in wheat. *Mol. Plant* **12**, 1639–1650 (2019).
19. Moore, J. W. et al. A recently evolved hexose transporter variant confers resistance to multiple pathogens in wheat. *Nat. Genet.* **47**, 1494–1498 (2015).
20. Kariola, T., Brader Gn, Li. J. & Palva, E. T. Chlorophyllase 1, a damage control enzyme, affects the balance between defense pathways in plants. *Plant Cell* **17**, 282–294 (2005).
21. Woodson Jesse, D., Perez-Ruiz Juan, M. & Chory, J. Heme synthesis by plastid ferrochelatase I regulates nuclear gene expression in plants. *Curr. Biol.* **21**, 897–903 (2011).
22. Mur, L. A. J. et al. Accumulation of chlorophyll catabolites photosensitizes the hypersensitive response elicited by *Pseudomonas syringae* in *Arabidopsis*. *N. Phytologist* **188**, 161–174 (2010).
23. Hirashima, M., Tanaka, R. & Tanaka, A. Light-independent cell death induced by accumulation of pheophorbide a in *Arabidopsis thaliana*. *Plant Cell Physiol.* **50**, 719–729 (2009).
24. Chen, H. et al. The Fd-GOGAT1 mutant gene lc7 confers resistance to *Xanthomonas oryzae* pv. *Oryzae* in rice. *Sci. Rep.* **6**, 26411 (2016).
25. Sakuraba, Y. et al. STAY-GREEN and chlorophyll catabolic enzymes interact at light-harvesting complex ii for chlorophyll detoxification during leaf senescence in *Arabidopsis*. *Plant Cell* **24**, 507–518 (2012).
26. Hörtensteiner, S. Stay-green regulates chlorophyll and chlorophyll-binding protein degradation during senescence. *Trends Plant Sci.* **14**, 155–162 (2009).
27. Wang, Y. et al. STAYGREEN, STAY HEALTHY: a loss-of-susceptibility mutation in the STAYGREEN gene provides durable, broad-spectrum disease resistances for over 50 years of US cucumber production. *N. Phytologist* **221**, 415–430 (2019).
28. Tang, C. et al. Functions of the lethal leaf-spot 1 gene in wheat cell death and disease tolerance to *Puccinia striiformis*. *J. Exp. Bot.* **64**, 2955–2969 (2013).
29. Clark, K. J., Pang, Z., Trinh, J., Wang, N. & Ma, W. Sec-delivered effector 1 (SDE1) of 'Candidatus Liberibacter asiaticus' promotes Citrus Huanglongbing. *Mol. Plant Microbe Interact.* **33**, 1394–1404 (2020).
30. Zhang, Y. et al. *Verticillium dahliae* secretory effector PevD1 induces leaf senescence by promoting ORE1-mediated ethylene biosynthesis. *Mol. Plant* **14**, 1901–1917 (2021).
31. Cao, W. et al. Suppressing chlorophyll degradation by silencing OsNYC3 improves rice resistance to *Rhizoctonia solani*, the causal agent of sheath blight. *Plant Biotechnol. J.* **20**, 335–349 (2022).
32. Borrill, P., Ramirez-Gonzalez, R. & Uauy, C. expVIP: a customizable RNA-seq data analysis and visualization platform. *Plant Physiol.* **170**, 2172–2186 (2016).
33. Xu, Q. et al. An effector protein of the wheat stripe rust fungus targets chloroplasts and suppresses chloroplast function. *Nat. Commun.* **10**, 5571 (2019).
34. De Brasi-Velasco, S. et al. Thioredoxin TRXo1 is involved in ABA perception via PYR1 redox regulation. *Redox Biol.* **63**, 102750 (2023).
35. Park, S. K. et al. Heat-shock and redox-dependent functional switching of an h-type *Arabidopsis* Thioredoxin from a disulfide reductase to a molecular chaperone. *Plant Physiol.* **150**, 552–561 (2009).
36. Arsova, B. et al. Plastidial Thioredoxin z interacts with two fructokinase-like proteins in a thiol-dependent manner: Evidence for an essential role in chloroplast development in *Arabidopsis* and *Nicotiana benthamiana*. *Plant Cell* **22**, 1498–1515 (2010).
37. Breen, S. et al. Chloroplasts play a central role in facilitating MAMP-triggered immunity, pathogen suppression of immunity and crosstalk with abiotic stress. *Plant, Cell Environ.* **45**, 3001–3017 (2022).
38. Zurbriggen, M. D. et al. Chloroplast-generated reactive oxygen species play a major role in localized cell death during the non-host interaction between tobacco and *Xanthomonas campestris* pv. *vesicatoria*. *Plant J.* **60**, 962–973 (2009).
39. Rodríguez-Herva, J. J. et al. A bacterial cysteine protease effector protein interferes with photosynthesis to suppress plant innate immune responses. *Cell. Microbiol.* **14**, 669–681 (2012).
40. Jelenska, J. et al. AJ domain virulence effector of *Pseudomonas syringae* remodels host chloroplasts and suppresses defenses. *Curr. Biol.* **17**, 499–508 (2007).
41. Wang, X. et al. Two stripe rust effectors impair wheat resistance by suppressing import of host Fe–S protein into chloroplasts. *Plant Physiol.* **187**, 2530–2543 (2021).
42. Rouhier, N. et al. Poplar Peroxiredoxin Q. A thioredoxin-linked chloroplast antioxidant functional in pathogen defense. *Plant Physiol.* **134**, 1027–1038 (2004).
43. Wang, P. et al. Evidence for a role of chloroplastic m-type thioredoxins in the biogenesis of Photosystem II in *Arabidopsis*. *Plant Physiol.* **163**, 1710–1728 (2013).
44. Geigenberger, P., Thormählen, I., Daloso, D. M. & Fernie, A. R. The unprecedented versatility of the plant thioredoxin system. *Trends Plant Sci.* **22**, 249–262 (2017).
45. Mukaihara, T., Hatanaka, T., Nakano, M. & Oda, K. *Ralstonia solanacearum* type III effector RipAY is a glutathione-degrading enzyme that is activated by plant cytosolic thioredoxins and suppresses plant immunity. *mBio* **7**, https://doi.org/10.1128/mbio.00359-00316 (2016).
46. Lorang, J. et al. Tricking the guard: Exploiting Plant defense for disease susceptibility. *Science* **338**, 659–662 (2012).
47. Jiang, Z. et al. Barley stripe mosaic virus γb protein targets thioredoxin h-type 1 to dampen salicylic acid-mediated defenses. *Plant Physiol.* **189**, 1715–1727 (2022).
48. Liu, Q. et al. An Atypical thioredoxin imparts early resistance to sugarcane mosaic virus in maize. *Mol. Plant* **10**, 483–497 (2017).
49. Mou, Z., Fan, W. & Dong, X. Inducers of plant systemic acquired resistance regulate NPR1 function through redox changes. *Cell* **113**, 935–944 (2003).
50. Tada, Y. et al. Plant immunity requires conformational charges of NPR1 via S-Nitrosylation and thioredoxins. *Science* **321**, 952–956 (2008).
51. Wan, A. & Chen, X. Virulence characterization of *Puccinia striiformis* f. sp. *tritici* using a new set of Yr single-gene line differentials in the United States in 2010. *Plant Dis.* **98**, 1534–1542 (2014).
52. Voegele, R. T., Struck, C., Hahn, M. & Mendgen, K. The role of haustoria in sugar supply during infection of broad bean by the rust fungus Uromyces fabae. *Proc. Natl Acad. Sci. USA* **98**, 8133–8138 (2001).
53. Fernandez, J., Marroquin-Guzman, M. & Wilson, R. A. Mechanisms of nutrient acquisition and utilization during fungal infections of leaves. *Annu. Rev. Phytopathol.* **52**, 155–174 (2014).
54. Berger, S., Sinha, A. K. & Roitsch, T. Plant physiology meets phytopathology: plant primary metabolism and plant–pathogen interactions. *J. Exp. Bot.* **58**, 4019–4026 (2007).
55. He, Z., Webster, S. & He, S. Y. Growth-defense trade-offs in plants. *Curr. Biol.* **32**, R634–R639 (2022).
56. Wang, J. et al. A single transcription factor promotes both yield and immunity in rice. *Science* **361**, 1026–1028 (2018).
57. Li, S. et al. Genome-edited powdery mildew resistance in wheat without growth penalties. *Nature* **602**, 455–460 (2022).
58. Sha, G. et al. Genome editing of a rice CDP-DAG synthase confers multipathogen resistance. *Nature* **618**, 1017–1023 (2023).

59. Kang, Z., Huang, L. & Buchenauer, H. Ultrastructural changes and localization of lignin and callose in compatible and incompatible interactions between wheat and *Puccinia striiformis* / *Ultrastrukturelle Veränderungen* und Lokalisierung von Lignin und Kailose in kompatiblen und inkompatiblen I. *Z. F.ür. Pflanzenkrankheiten Und Pflanzenschutz* **109**, 25–37 (2002).
60. Ma, S. et al. WheatOmics: A platform combining multiple omics data to accelerate functional genomics studies in wheat. *Mol. Plant* **14**, 1965–1968 (2021).
61. Zhang, Z. et al. Development of an *Agrobacterium*-delivered CRISPR/Cas9 system for wheat genome editing. *Plant Biotechnol. J.* **17**, 1623–1635 (2019).
62. Wang, N. et al. Inactivation of a wheat protein kinase gene confers broad-spectrum resistance to rust fungi. *Cell* **185**, 2961–2974.e2919 (2022).
63. Zhang, R. et al. The RING-finger ubiquitin E3 ligase TaPIR1 targets TaHRP1 for degradation to suppress chloroplast function. *Nat. Commun.* **15**, 6905 (2024).
64. Hu, S. et al. Deacetylation of chitin oligomers by *Fusarium graminearum* polysaccharide deacetylase suppresses plant immunity. *Mol. Plant Pathol.* **24**, 1495–1509 (2023).
65. Xu, Q. et al. The N-terminus of a *Fusarium graminearum*-secreted protein enhances broad-spectrum disease resistance in plants. *Mol. Plant Pathol.* **23**, 1751–1764 (2022).
66. Kim, D., Langmead, B. & Salzberg, S. L. HISAT: a fast spliced aligner with low memory requirements. *Nat. Methods* **12**, 357–360 (2015).
67. Petre, B. et al. Rust fungal effectors mimic host transit peptides to translocate into chloroplasts. *Cell. Microbiol.* **18**, 453–465 (2016).
68. Park, S.-Y. et al. The senescence-induced staygreen protein regulates chlorophyll degradation. *Plant cell* **19**, 1649–1664 (2007).
69. Benedetti, C. E. & Arruda, P. Altering the expression of the chlorophyllase gene ATHCOR1 in transgenic *Arabidopsis* caused changes in the chlorophyll-to-chlorophyllide ratio. *Plant Physiol.* **128**, 1255–1263 (2002).
70. Arnon, D. I. Copper enzymes in isolated chloroplasts. Polyphenoloxidase in *Beta Vulgaris*. *Plant Physiol.* **24**, 1–15 (1949).

Acknowledgements

We thank Prof. Qixin Sun and Mingming Xin (China Agricultural University) for providing pBUE411 vector used in this study. This study was supported by the National Natural Science Foundation of China (32225041, X.J.W.; 32102229, Q.X.), the Sichuan Science and Technology Program (2024NSFSC0405, Q.X.; 2021YJ0298, Q.X.), China Agriculture Research System (CARS-3, X.J.W.), and the Biotech Breeding Program of State Key Laboratory of Crop Gene Exploration and Utilization in Southwest China (SKL-ZY202233, Q.X.).

Author contributions

Q.X., Y.M.W., X.R.Q. and Y.L. coordinated the research and designed the experiments. Y.L. and X.R.Q. performed the majority of the experiments. Q.W. and W.J.Y. performed the histological observation and plasmids construction. X.R.Q. cultured tobacco and wheat plants. X.D.W. and X.R.Q. performed the subcellular localization assay. J.M, Y.Z.Z., G.Y.C., P.F.Q., Q.T.J and Y.L.Z. provided technical support. Q.X., Y.M.W., and X.J.W. wrote and revised the paper.

Competing interests

The authors declare no competing interests.

Additional information

Supplementary information The online version contains supplementary material available at https://doi.org/10.1038/s41467-025-58277-5.

Correspondence and requests for materials should be addressed to Xiaojie Wang, Yuming Wei or Qiang Xu.

Peer review information *Nature Communications* thanks the anonymous reviewer(s) for their contribution to the peer review of this work. A peer review file is available.